# Extensive *HST* Ultraviolet Spectra and Multi-wavelength Observations of SN 2014J in M82 Indicate Reddening and Circumstellar Scattering by Typical Dust

Ryan J. Foley[1,2]⋆, O. D. Fox[3], C. McCully[4], M. M. Phillips[5], D. J. Sand[6], W. Zheng[3], P. Challis[7], A. V. Filippenko[3], G. Folatelli[8], W. Hillebrandt[9], E. Y. Hsiao[5], S. W. Jha[4], R. P. Kirshner[7], M. Kromer[10], G. H. Marion[11], M. Nelson[12], R. Pakmor[13], G. Pignata[14,15], F. K. Röpke[16], I. R. Seitenzahl[17], J. M. Silverman[11], M. Skrutskie[12], M. D. Stritzinger[18]

[1] *Astronomy Department, University of Illinois at Urbana–Champaign, 1002 W. Green Street, Urbana, IL 61801, USA*
[2] *Department of Physics, University of Illinois Urbana–Champaign, 1110 W. Green Street, Urbana, IL 61801, USA*
[3] *Department of Astronomy, University of California, Berkeley, CA 94720-3411, USA*
[4] *Department of Physics and Astronomy, Rutgers, the State University of New Jersey, 136 Frelinghuysen Road, Piscataway, NJ 08854, USA*
[5] *Carnegie Observatories, Las Campanas Observatory, La Serena, Chile*
[6] *Physics Department, Texas Tech University, Lubbock, TX 79409, USA*
[7] *Harvard-Smithsonian Center for Astrophysics, 60 Garden Street, Cambridge, MA 02138, USA*
[8] *Kavli Institute for the Physics and Mathematics of the Universe, Todai Institutes for Advanced Study, the University of Tokyo, Kashiwa, Japan 277-8583 (Kavli IPMU, WPI)*
[9] *Max-Planck-Institut für Astrophysik, Karl-Schwarzschild-Strasse 1, D-85748 Garching bei München, Germany*
[10] *The Oskar Klein Centre & Department of Astronomy, Stockholm University, AlbaNova, SE-106 91 Stockholm, Sweden*
[11] *Department of Astronomy, University of Texas, Austin, TX 78712-0259, USA*
[12] *Department of Astronomy, University of Virginia, Charlottesville, VA 22904, USA*
[13] *Heidelberger Institut für Theoretische Studien, Schloss-Wolfsbrunnenweg 35, D-69118 Heidelberg, Germany*
[14] *Departamento de Ciencias Fisicas, Universidad Andres Bello, Avda. Republica 252, Santiago, Chile*
[15] *Millennium Institute of Astrophysics, Avda. Republica 252, Santiago, Chile*
[16] *Institut für Theoretische Physik und Astrophysik, Universität Würzburg, Emil-Fischer-Str. 31, D-97074 Würzburg, Germany*
[17] *Research School of Astronomy and Astrophysics, Mount Stromlo Observatory, Cotter Road, Weston Creek, ACT 2611, Australia*
[18] *Department of Physics and Astronomy, Aarhus University, Ny Munkegade, DK-8000 Aarhus C, Denmark*

*arXiv:1405.3677v2 [astro-ph.HE] 14 Jul 2014*

**ABSTRACT**

SN 2014J in M82 is the closest detected Type Ia supernova (SN Ia) in at least 28 years and perhaps in 410 years. Despite its small distance of 3.3 Mpc, SN 2014J is surprisingly faint, peaking at $V = 10.6$ mag, and assuming a typical SN Ia luminosity, we infer an observed visual extinction of $A_V = 2.0 \pm 0.1$ mag. But this picture, with $R_V = 1.6 \pm 0.2$, is too simple to account for all observations. We combine 10 epochs (spanning a month) of *HST*/STIS ultraviolet through near-infrared spectroscopy with *HST*/WFC3, KAIT, and FanCam photometry from the optical to the infrared and 9 epochs of high-resolution TRES spectroscopy to investigate the sources of extinction and reddening for SN 2014J. We argue that the wide range of observed properties for SN 2014J is caused by a combination of dust reddening, likely originating in the interstellar medium of M82, and scattering off circumstellar material. For this model, roughly half of the extinction is caused by reddening from typical dust ($E(B - V) = 0.45$ mag and $R_V = 2.6$) and roughly half by scattering off LMC-like dust in the circumstellar environment of SN 2014J.

**Key words:**  dust, extinction – galaxies: individual: M82 – supernovae: general – supernovae: individual: SN 2014J

---

⋆ E-mail:rfoley@illinois.edu

# 1 INTRODUCTION

Type Ia supernovae (SNe Ia) are rare enough that nearby SNe Ia ($D < 5$ Mpc) are discovered only about once a decade. But these rare events, which provide unique and extremely high-quality data and can be monitored for years, can lead to large jumps in our understanding of SN physics.

Observations of SNe Ia were used to discover the accelerating expansion of the Universe (Riess et al. 1998; Perlmutter et al. 1999), and they continue to be one of our best cosmological probes (e.g., Rest et al. 2013; Betoule et al. 2014).

One of the largest potential systematic uncertainties for using SNe Ia as cosmological probes is the poorly constrained and potentially peculiar properties of absorbing dust along the line of sight to SNe Ia (e.g., Scolnic et al. 2013, 2014). Understanding these dust properties, often simplified as a single reddening-law parameter, $R_V$, is critical for cosmological measurements since the distance modulus measured to a SN Ia is

$$\mu = m_V - M_V + E(B-V) \cdot R_V, \tag{1}$$

where $m_V$ and $M_V$ are the apparent and absolute magnitudes of a SN in the $V$ band, $E(B-V)$ is the reddening, and $R_V$ is the ratio of the total-to-selective extinction. Similar equations exist for all bands.

Several different methods indicate that the dust reddening SNe Ia has $R_V < 2$, which is significantly below the average value — and below nearly the entire population — for Milky Way lines of sight (e.g., Fitzpatrick & Massa 2007). SN reddening is measured by comparing observed SN colours to a zero-reddening locus (e.g., Riess et al. 1996; Phillips et al. 1999). Various methods of examining large samples of SNe Ia have resulted in $R_V < 2$ (e.g., Nobili et al. 2005; Guy et al. 2005; Hicken et al. 2009b; Folatelli et al. 2010; Burns et al. 2011). It is now understood that at least part of the reason for the low values of $R_V$ from large samples is because of poor assumptions about the intrinsic colour distribution of SNe Ia (e.g., Foley & Kasen 2011; Mandel et al. 2011); correcting for this effect can increase the best-fitting $R_V$ from 1.6 to 2.5 for a large sample of SNe Ia (Foley & Kasen 2011). However, there are several examples of highly reddened SNe Ia, where $R_V$ can be measured directly, that still have $R_V < 2$ (e.g., Elias-Rosa et al. 2006, 2008; Krisciunas et al. 2006; Wang et al. 2008).

As an alternative to the Milky Way having peculiar dust, Wang (2005) suggested that circumstellar dust scattering will naturally lead to low values of $R_V$. Presumably SNe Ia with higher reddening are more likely to have additional, circumstellar dust, which can potentially both scatter and redden, perhaps resolving the low values of $R_V$ for the most highly reddened SNe Ia. Patat et al. (2006) further investigated this possibility providing several predictions for observations. Goobar (2008, hereafter, G08) quantified this effect, producing simulations of how the scattering will affect a SN spectral energy distribution (SED) and the inferred $R_V$.

Adding further mystery to the situation are correlations between SN observables and gas/dust properties. Specifically, highly reddened SNe Ia with high-velocity ejecta tend to have lower values for $R_V$ relative to their equally reddened, low ejecta velocity counterparts (Wang et al. 2009).

Additionally, SNe Ia that have statistical evidence for circumstellar gas (as well as those with variable narrow absorption features which provide strong evidence for circumstellar gas) also have higher ejecta velocities on average (Foley et al. 2012c). These results indicate that the progenitor system or possibly orientation effects are related to the inferred dust properties.

## 1.1 SN 2014J

SN 2014J was discovered at an $R$-band magnitude of 10.5 on 2014 Jan 21.805 (UT dates are used throughout this paper) by Fossey et al. (2014). After its initial discovery, multiple groups reported pre-discovery detections and limits (e.g., Denisenko et al. 2014; Dhungana et al. 2014; Gerke et al. 2014; Ma et al. 2014; Zheng et al. 2014). The SN was promptly spectroscopically identified as a young SN Ia (Ayani 2014; Cao et al. 2014; Itoh et al. 2014). We triggered multiple programs to study the photometric and spectroscopic evolution of the SN, its circumstellar environment, its polarisation, its energetics, and other aspects. In particular, we triggered our *Hubble Space Telescope* (*HST*) target-of-opportunity program to obtain ultraviolet (UV) spectra of SNe Ia (GO-13286; PI Foley; Foley 2014).

SN 2014J, in M82, is the nearest SN Ia in at least 28 years. Our best distance estimate of M82 (Section 3.2) is $D = 3.3$ Mpc, placing SN 2014J formally closer than SNe 1972E and 1986G ($D = 3.6$ and 3.7 Mpc), but uncertainties in the distance measurements currently prevent a definitive ranking. However, if these measurements are accurate, SN 2014J is the nearest detected SN Ia since Kepler's SN (410 years).

Being so close, SN 2014J has been observed extensively at many wavelengths. Zheng et al. (2014) presented early optical photometry of SN 2014J, constraining the explosion time. Nondetections in X-rays (Margutti et al. 2014) and radio (Chandler & Marvil 2014; Chandra et al. 2014; Chomiuk et al. 2014) provide no evidence for a dense and smooth circumstellar environment. Pre-explosion optical images with no luminous source at the position of SN 2014J are inconsistent with red supergiant companion stars (Goobar et al. 2014; Kelly et al. 2014), while nondetections in pre-explosion X-ray images are inconsistent with the progenitor system being in a super-soft state in the decade before explosion (Maksym et al. 2014; Nielsen et al. 2014).

Spectropolarimetric observations of SN 2014J were made to directly constrain $R_V$ by measuring the wavelength of maximum polarisation (Patat et al. 2014), indicating $R_V < 2$. High-resolution spectroscopy has revealed a multitude of interstellar and/or circumstellar absorption features (Welty et al. 2014), which have been used to detect circumstellar material (CSM) in other SNe Ia (Patat et al. 2007; Blondin et al. 2009; Simon et al. 2009).

Goobar et al. (2014) presented optical and near-infrared (NIR) photometry, several low-resolution optical spectra, and a high-resolution spectrum. Examining their light curves and spectra, they determine that a simple reddening law with $R_V \approx 1.4$ provides a good match to their data. Marion et al. (2014), with similar data, came to similar conclusions. Recently, Amanullah et al. (2014) added more photometry, covering more bands and a longer time baseline to the Goobar et al. (2014) photometry, and also found

a best-fitting value of $R_V = 1.4 \pm 0.1$ for a simple dust reddening law. They also found that a power-law reddening law with an index of $-2.1 \pm 0.1$ is consistent with the data.

In this manuscript, we present our UV, optical, and NIR data in Section 2. The extinction to SN 2014J is estimated in Section 3. We describe dust reddening and circumstellar scattering models in Section 4, and we use those models to estimate the reddening of SN 2014J based on our photometry (Section 5) and spectroscopy (Section 6). We discuss our findings and summarize our conclusions in Section 7.

## 2 OBSERVATIONS

### 2.1 Photometry

SN 2014J in M82 was observed with *HST*/WFC3 UVIS over 7 epochs between 2014 January 28 and 2014 March 07 (DD-13621; PI Goobar). All 7 epochs include observations in the F218W, F225W, F275W, and F336W filters. Epochs 1 and 3 include observations in the F467M, F631N, and F845M filters. Epochs 2, 4, 5, and 6 include observations in F438W, F555W, and F814W (roughly *B*, *V*, and *I*).

We combined exposures and performed cosmic-ray rejection using AstroDrizzle after we performed the pixel-based charge-transfer efficiency correction. We registered the individual flatfielded (flt) frames using TweakReg in DrizzlePac. In the images, the SN was the only detected object, so we did not attempt to register the absolute astrometry or perform background subtraction.

An image combining *HST*/WFC3 observations of SN 2014J with deep pre-explosion images of M82 is shown in Figure 1. To create this image, we obtained images of M82 from the Hubble Legacy Archive observed in the F435W, F555W, F658N, and F814W filters (roughly *B*, *V*, H$\alpha$, and *I*), with exposure times of 10,800, 8160, 26,400, and 4200 s, respectively. Conversely, the SN images are extremely short (0.48 s). While this choice prevents saturated images, the short exposure times also prevent an accurate characterisation of the wings of the point-spread function (PSF). As such, a simple combination of the pre-explosion and SN images causes the SN to appear much fainter to the human eye than its true brightness. Instead, we injected a model PSF, generated using Tiny Tim (Krist et al. 2011), at the location of the SN with the measured brightness in each band. We then combined the final images with F435W, F555W, and F658N + F814W as the blue, green, and red channels. SN 2014J still appears somewhat faint in Figure 1 because of the excellent *HST* PSF. To see faint structures in M82, we chose a dynamic range which saturates the SN.

We performed aperture photometry on the SN using the APPHOT package in IRAF[1]. For each image, we used a $0''.4$ aperture. For the last epoch in F218W and the last two epochs of F275W, the SN had faded enough such that using such a large aperture was introducing a systematic bias into our results. To account for this, we measured the photometry for a 5-pixel ($0''.2$) aperture and used aperture corrections derived from the earlier epochs to convert to the $0''.4$ aperture. Our photometric uncertainties include the reported uncertainty from Phot (assuming a read-noise contribution of 3.15 electrons) and the uncertainty from the aperture correction added in quadrature. The uncertainty in the aperture correction was taken to be the standard deviation of the measurements from the early epochs.

We list all *HST* photometry in Table 1, but we only include the F218W, F225W, F275W, and F336W data in our analysis. The other filters overlap with other bands which have more complete temporal coverage.

The *HST* images were independently reduced and analysed by Amanullah et al. (2014). Comparing our measurements with those listed in that work, we find the photometry to be consistent within the quoted uncertainties.

Filtered CCD images of SN 2014J were obtained with the 0.76-m Katzman Automatic Imaging Telescope (KAIT; Filippenko et al. 2001) at Lick Observatory All KAIT images were reduced using our image-reduction pipeline (Ganeshalingam et al. 2010). PSF photometry was then performed using DAOPHOT (Stetson 1987). The SN instrumental magnitudes have been calibrated to two nearby stars from the APASS catalogue[2]. The APASS magnitudes are transformed into the Landolt system[3] before they are used for calibrating KAIT data. Owing to the lack of template images prior to the SN explosion, we have not performed image subtraction. Consequently, the photometry presented here should be considered preliminary; however, because SN 2014J is much brighter than its surrounding regions and the pre-explosion *HST* images do not indicate a bright region coincident with SN 2014J, the background contamination should be minimal for all epochs presented here. Table 2 lists the KAIT photometry.

NIR ($JHK_s$) observations were made with FanCam, a 1024×1024 pixel HAWAII-I HgCdTe imaging system (Kanneganti et al. 2009) on the University of Virginia's 31-inch telescope at Fan Mountain, just outside of Charlottesville, VA. Observations consist of a series of either 4, 8, or 10 s integrations. We employed standard NIR data-reduction techniques in IRAF. The brightest parts of M82 can be fit into a single array quadrant, so that dithering can efficiently utilise empty quadrants as sky exposures. Each quadrant was reduced separately and, ultimately, coadded into a single image. The data were analysed with the online astrometry programs SEXTRACTOR and SWARP. Calibration was performed using field stars with reported fluxes in the Two Micron All Sky Survey (2MASS; Skrutskie et al. 2006). Table 3 lists the NIR photometry.

We report photometric parameters (times of maximum brightness, peak brightness, decline rate) in Table 7. Importantly, we measure $t_{\max}(B) = 2,456,690.5 \pm 0.2$ (JD), $V_{\max} = 10.61 \pm 0.05$ mag, and $\Delta m_{15}(B) = 0.95 \pm 0.01$ mag. Our computed values are consistent with those of Tsvetkov et al. (2014) and Marion et al. (2014). We caution that these are the observed values and are uncorrected for reddening.

---

[1] IRAF: the Image Reduction and Analysis Facility is distributed by the National Optical Astronomy Observatory, which is operated by the Association of Universities for Research in Astronomy (AURA) under cooperative agreement with the National Science Foundation (NSF).

[2] http://www.aavso.org/apass/
[3] http://www.sdss.org/dr7/algorithms/sdssUBVRITransform.html#Lupton2005.

**Figure 1.** *HST*/WFC3 image of SN 2014J in M82. The RGB channels correspond to F658N+F814W, F555W, and F435W (roughly Hα+*IVB*), respectively. Because the *HST* images of SN 2014J do not probe the wings of the PSF in the same way as the deep M82 pre-explosion image, simple stacking of the pre-explosion M82 and SN 2014J images produces an image where SN 2014J appears fainter than it should. Using the brightness measurements of SN 2014J in these bands, an artificial star was generated with Tiny Tim to match the PSF of the deep, wide-field M82 image. This source was inserted at the position of SN 2014J to create an accurate visualisation.

All photometry is presented in Tables 1 – 3 and the subset used for our analysis is shown in Figure 2.

## 2.2 Spectroscopy

SN 2014J was observed by *HST* using the STIS spectrograph on ten epochs from 2014 January 26.60 to 2014 February 26.07, corresponding to $t = -6.4$ to 24.1 days relative to *B*-band maximum. Each individual spectrum was obtained over two to five orbits with the $52'' \times 0.''2$ slit and three different setups: the near-UV MAMA detector and the G230L grating, the CCD/G430L, and the CCD/G750L. The three setups yield a combined wavelength range of 1615–10,230 Å. A log of observations is presented in Table 4.

The data were reduced using the standard *HST* Space Telescope Science Data Analysis System (STSDAS) routines to bias subtract, flatfield, extract, wavelength-calibrate, and flux-calibrate each SN spectrum. The spectra are presented in Figure 3.

Ground-based NIR spectroscopy of SN 2014J was obtained by the NASA Infrared Telescope Facility (IRTF) with SpeX (Rayner et al. 2003) in cross-dispersed mode and a $0.''3$ slit, which yields 0.8–2.5 $\mu$m wavelength coverage at $R = 2000$. All observations were taken utilising the standard ABBA technique, with the slit oriented along the parallactic angle. A telluric standard with a A0V spectral type was observed for flux calibration and telluric correction. The data reductions made use of the Spextool and XTELLCOR software packages (Vacca et al. 2003; Cushing et al. 2004).

A log of observations is presented in Table 5. These data are also presented by Marion et al. (2014).

High-dispersion optical spectroscopy of SN 2014J was obtained with the Tillinghast Reflection Echelle Spectrograph (TRES; Füresz 2008) on the Tillinghast 1.5 m telescope at the Fred Lawrence Whipple Observatory. TRES is a fiber-fed, crossed-dispersed spectrograph covering the wavelength range 3850–9100 Å with some gaps at wavelengths beyond 6650 Å. Ten observations of SN 2014J were made between 23 January 2014 and 22 March 2014 employing a 100 $\mu$m (2.3 ") fiber giving $R = 30,000$. A log of observations is presented in Table 6.

## 3 EXTINCTION ESTIMATES

Extinction and reddening measurements are well defined for stars and galaxies, but SNe, with their broad spectral features, require more attention to detail. Here we define some necessary terms for comprehending our results.

For an extinction ($A_X$), colour excess ($E(X - Y)$), or the ratio of the total-to-selective extinction ($R_\lambda$), there are observed and "true" quantities. The observed quantities are defined as

$$A_X^{\mathrm{obs}} \equiv X^{\mathrm{obs}} - X^{\mathrm{no\ red}}, \qquad (2)$$

$$E(X - Y)^{\mathrm{obs}} \equiv A_X^{\mathrm{obs}} - A_Y^{\mathrm{obs}}, \text{ and} \qquad (3)$$

$$R_V^{\mathrm{obs}} \equiv A_V^{\mathrm{obs}}/E(B - V)^{\mathrm{obs}}, \qquad (4)$$

where $X^{\mathrm{no\ red}}$ and $X^{\mathrm{obs}}$ are the brightness of the SN in
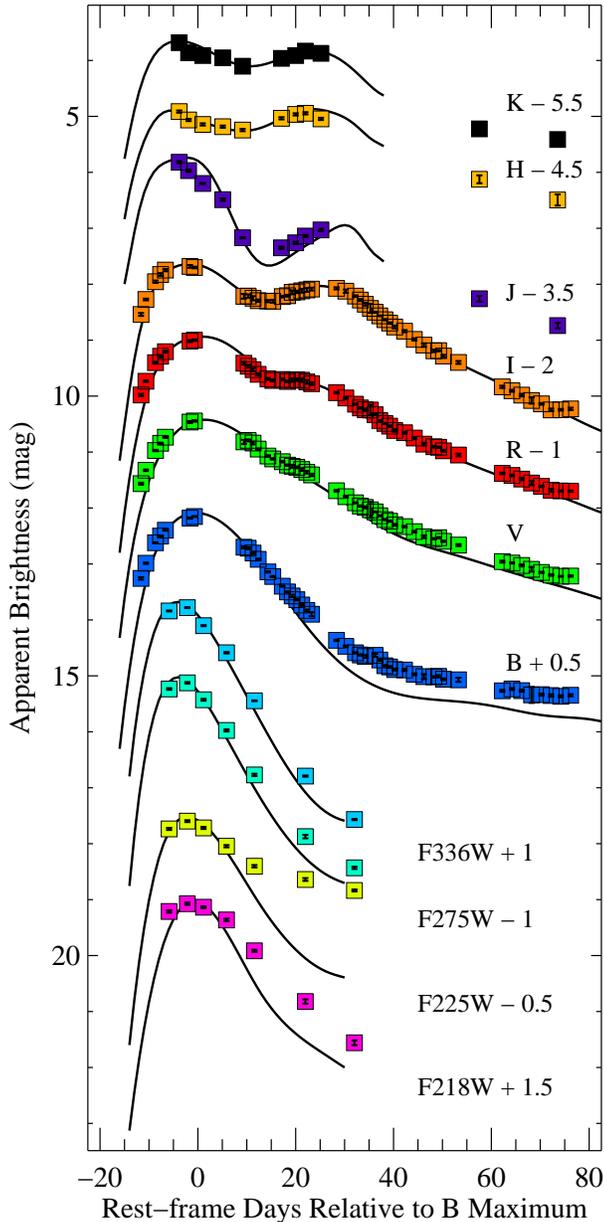
**Figure 2.** *HST*/WFC3, KAIT, and FanCam "UV," optical, and NIR light curves of SN 2014J (squares). Overplotted are the optical and NIR light curves of SN 2011fe (black curves; Matheson et al. 2012; Richmond & Smith 2012), and the synthesised UV light curves from the SN 2011fe *HST* spectra, shifted to match the peak brightness of SN 2014J in each band.



**Figure 3.** *HST*/STIS spectral time series of SN 2014J. The phase relative to *B*-band maximum brightness is labeled. The spectra have been dereddened only by the Milky Way reddening estimate.

in the effective wavelength of photometric filters with increased reddening (Section 5.2), spectroscopy is preferred for disentangling the differences between observed and true parameters.

### 3.1 Milky Way Reddening

The nominal Milky Way reddening toward M82, as determined by Schlafly & Finkbeiner (2011) from Schlegel et al. (1998) dust maps, is $E(B - V) = 0.138$ mag. This value is used by Goobar et al. (2014) and several other studies of SN 2014J. Dalcanton et al. (2009) note that M82 is a strong source in the dust maps, biasing the reddening measurement. They instead suggest a value of $E(B - V) = 0.061$ mag as determined from regions surrounding M82. This value is used by Amanullah et al. (2014). However, the Dalcanton et al. (2009) estimate is on the Schlegel et al. (1998) scale; converting to the Schlafly & Finkbeiner (2011) scale, the Milky Way reddening is $E(B - V) = 0.054$ mag, which we use in this work.

### 3.2 Direct Measurement

SNe Ia are standardisable candles in the optical and nearly standard candles in the NIR. One can directly measure the extinction to SN 2014J from measuring its distance and brightness.

the $X$ band without any extinction and as observed, respectively.

Meanwhile, $E(X - Y)^{\text{true}}$ and $R_V^{\text{true}}$ are the reddening and the ratio of total-to-selective extinction, respectively, required such that dereddening the observed spectrum of the SN results in a spectrum equivalent to the unreddened spectrum.

One can convert from the observed and true quantities by knowing the underlying SED of the SN (e.g., Phillips et al. 1999; Nugent et al. 2002). Because of a shift

The distance to M82 is measured with moderate precision. Parallel observations of our STIS UV campaign were conducted to find and measure distances from Cepheids in M82. These data will be presented elsewhere, but should provide a precise distance estimate for the galaxy.

NED lists 7 distance estimates (with uncertainties) from 3 methods, ranging from $\mu = 27.53 \pm 0.05$ mag (Dalcanton et al. 2009) to $\mu = 28.57 \pm 0.80$ mag (Tully 1988). There are large discrepancies even from the same methods and authors. For instance, Dalcanton et al. (2009) measured tip of the red giant branch (TRGB) distances of $\mu = 27.53 \pm 0.05$ and $27.74 \pm 0.04$ for two positions in the galaxy. These measurements are discrepant at the $3.3\sigma$ level and correspond to a distance difference of 320 kpc. M82 is in the M81 group and is interacting with M81 (Yun et al. 1994), which has a Cepheid distance of $\mu = 27.60 \pm 0.03$ mag (Gerke et al. 2011).

For the NIR bands, SNe Ia are nearly standard candles (Krisciunas et al. 2004; Wood-Vasey et al. 2008; Mandel et al. 2009; Folatelli et al. 2010; Burns et al. 2011; Kattner et al. 2012). SN 2014J appears to have a normal decline rate, further indicating that it will have a standard peak luminosity at these wavelengths. Using the $K$-band light curve of SN 2014J, the suite of peak $K$-band absolute magnitudes listed by Matheson et al. (2012), and *no* extinction in M82, we find a weighted average distance modulus of $\mu = 27.57 \pm 0.13$ mag and a limit of $\mu < 27.60 \pm 0.08$ mag[4]. This value is only consistent with the closest distances measured for M82. For reasonable assumptions about the reddening and extinction law for SN 2014J, we expect the extinction in the $K$ band, $A_K$, to be $\lesssim 0.05$–0.15 mag, but any extinction in the $K$ band will further decrease the distance modulus. We therefore assume $\mu = 27.60$ mag, a value consistent with the $K$-band SN 2014J measurements, the M81 Cepheid distance, and the closer direct distance measurements of M82. We adopt an uncertainty of 0.10 mag, which is reasonable for the set of distances that are allowed by the $K$-band data.

We measure the peak brightness of SN 2014J in all bands, and these are reported in Table 7. Using the peak absolute magnitudes from Prieto et al. (2006) and the suite of measurements collated by Matheson et al. (2012) for the optical and NIR, respectively, we measure the extinction in each band, also listed in Table 7. Assuming that SN 2014J had a typical SN Ia luminosity, we find the observed visual extinction to be $A_V^{\rm obs} = 2.07 \pm 0.18$ mag at maximum brightness.

### 3.3    Extinction from Optical-Infrared Colours

The extinction in band $X$ ($A_X$) is essentially equivalent to $E(X - Y)$ for cases where $A_Y^{\rm obs} \approx A_Y^{\rm true} \approx 0$ mag. If $A_Y$ is negligible, then this measurement is independent of distance. As shown above, $A_K \approx 0$ mag for reasonable assumptions for the distance, and therefore $A_V^{\rm obs} \approx E(V - K)^{\rm obs}$.

---

[4] We have no data before maximum in the NIR bands, but do cover the time of $B$-band maximum brightness. Some methods measure the absolute magnitude at peak in a given band, for which we only have limits, while others measure the absolute magnitude at the time of $B$-band maximum brightness.

Using a Cardelli et al. (1989) reddening law with $R_V = 3.1$, $A_V^{\rm obs} = 1.14 E(V - K)^{\rm obs}$. We provide detailed measurements of $E(V - K)$ in Section 5.3. Using the average reddening, we estimate $A_V^{\rm obs} = 1.91 \pm 0.10$ mag.

We similarly determined that $A_H^{\rm obs}$ should be low (0.13 mag), and we measure an average reddening of $E(V - H)^{\rm obs} = 1.77 \pm 0.12$ mag. Therefore, $A_V^{\rm obs} = E(V - H)^{\rm obs} + A_H^{\rm obs} = 1.91$ mag is consistent with our earlier measurements.

From multiple methods, we determine that there is $A_V^{\rm obs} = 1.95 \pm 0.09$ mag of host-galaxy extinction along the line of sight to SN 2014J. Because of our methodology, this measurement is only valid at maximum brightness. Using the same methods, we measure $A_B^{\rm obs} = 3.14 \pm 0.11$ mag. Therefore, from model-independent methods, we determine a maximum-brightness reddening of $E(B - V)^{\rm obs} \equiv A_B^{\rm obs} - A_V^{\rm obs} = 1.19 \pm 0.14$ mag and $R_V^{\rm obs} \equiv A_V^{\rm obs}/E(B - V)^{\rm obs} = 1.64 \pm 0.16$.

### 3.4    Extinction from High-resolution Spectroscopy

As discussed by Welty et al. (2014), the spectrum of SN 2014J displayed strong, complex interstellar absorption lines of Na I, K I, Ca I, Ca II, CH, CH+, and CN, as well as a number of diffuse interstellar bands (DIBs). Welty et al. interpreted the strong absorption at velocities $v_{\rm LSR} > 30$ km s$^{-1}$ as arising in the interstellar medium (ISM) of M82. We have used the TRES spectra of SN 2014J, which cover the phases from $-9.6$ to $+45.3$ days with respect to the epoch of $B$-band maximum brightness, to look for possible variability of the DIBs at 5870 Å and 5797 Å, and the Na I D and K I $\lambda 7665$ absorption complexes.

The equivalent widths of the DIBs were calculated using the IRAF task `fitprofs` assuming Gaussian profiles of 2.8 Å full width at half-maximum intensity (FWHM) and 2.0 Å FWHM, respectively. The measurements are displayed in Figure 4. No variability is detected for either DIB over the period of the observations. Using all data, we find weighted mean equivalent widths of EW(5780) $= 344 \pm 21$ mÅ and EW(5797) $= 229 \pm 10$ mÅ. These numbers are for the combined Milky Way + M82 absorption since it is not possible to separate them. However, as discussed by Welty et al., the Milky Way contribution is expected to be small ($\sim$ 5%). Our measurements are in excellent agreement with those of Welty et al., but the EW(5780) value quoted by Goobar et al. (2014) of $480 \pm 10$ mÅ from high-dispersion spectra obtained on 26 January 2014 and 28 January 2014 (UT) ($-6$ and $-4$ days with respect to $B$ maximum) differs by $5.8\sigma$. Using our measurement of EW(5780), a total visual extinction of $A_V = 1.8 \pm 0.9$ mag is inferred from Equation 6 of Phillips et al. (2013).

Figure 5 shows the evolution of the Na I D absorption in SN 2014J from $-9.6$ to $+18.4$ days with respect to $B$-band maximum brightness. (The final two TRES spectra obtained 1.5 months after $B$ maximum are not included in this figure owing to their lower S/N.) The telluric absorption features at these wavelengths are also indicated. No credible evidence is seen in the Na I D lines for variations of any of the absorption components, although the strongly saturated absorption at $+60 > v_{\rm LSR} > +150$ km s$^{-1}$ would make small variations in this velocity range difficult to discern. The weaker K I $\lambda\lambda 7665, 7699$ lines are much more useful for
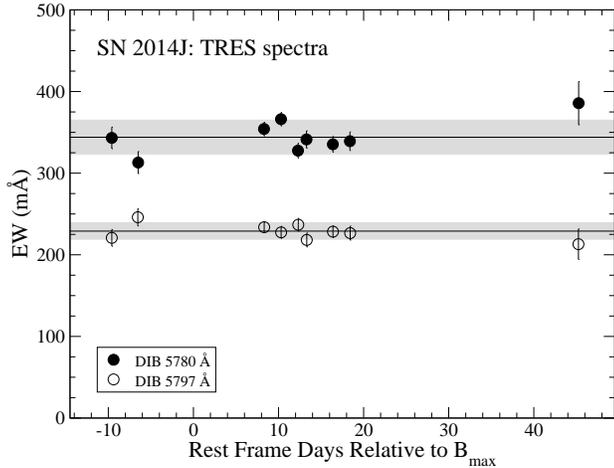
**Figure 4.** Equivalent-width measurements of the DIB features at 5780 Å and 5797 Å in the spectra of SN 2014J plotted as a function of light-curve phase. The horizontal lines and grey regions represent the mean and $1\sigma$ scatter for each feature. As noted in the text, these measurements are for the combined Milky Way + M82 absorption. The final points at +45 days were measured from the sum of the spectra obtained on 2014 March 16 and 2014 March 22.
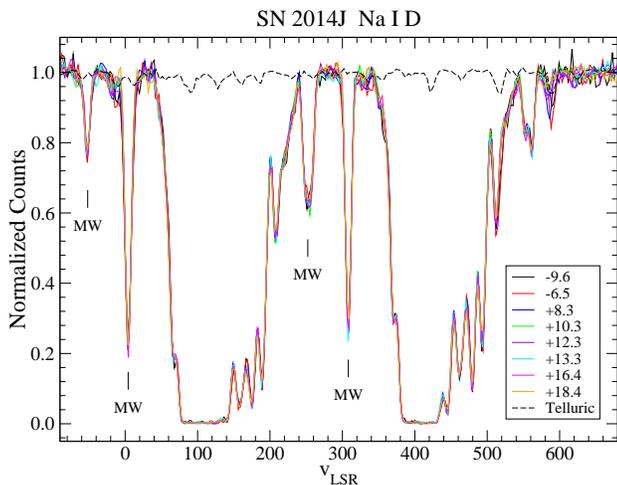


**Figure 5.** Normalised profiles of the Na I D line absorption in SN 2014J from −9.6 to +18.4 days with respect to the epoch of $B$-band maximum brightness. The different epochs have different colours and are labeled. The telluric spectrum, as measured from a hot star, is plotted as a dashed line. The absorption components likely associated with Milky Way gas are marked. The remaining absorption is likely from the ISM of M82 or the CSM of SN 2014J.

exploring these absorption components. Our TRES spectra, which covered the 7665 Å line only, also show no evidence for variations.

## 4 REDDENING/SCATTERING MODELS

To further understand the reddening and scattering properties of SN 2014J, we apply specific models to our photo-

metric and spectroscopic data. We have chosen 6 models to test, as follows.

- **CCM31** A Cardelli et al. (1989, hereafter, CCM) reddening law as modified by O'Donnell (1994) with $R_V = 3.1$, the canonical Milky Way value.
- **F9931**: A Fitzpatrick (1999, hereafter, F99) reddening law with $R_V = 3.1$.
- **CCM**: A Cardelli et al. (1989) reddening law as modified by O'Donnell (1994) with no restriction on $R_V$.
- **F99**: A Fitzpatrick (1999) reddening law with no restriction on $R_V$. The values reported here use the Milky Way dust parameters for this reddening law. We also fit the data with an LMC reddening law, which typically changed any parameter by <2%.
- **CSM**: A circumstellar material scattering model as described by G08. Here the reddening is described by a power law.
- **CSMD**: A two-component model with both a circumstellar scattering component and a F99 dust reddening component.

The scattering of SN photons off circumstellar dust should alter the observed light curves and spectra from SNe Ia (Wang 2005; Patat et al. 2006; Goobar 2008; Amanullah & Goobar 2011). G08 simulated this effect and determined the effects on the observed extinction,

$$\frac{A_\lambda}{A_V} = 1 - a + a \left( \frac{\lambda}{\lambda_V} \right)^p, \qquad (5)$$

where $\lambda_V$ is the wavelength of the $V$ band (chosen to be 5500 Å by G08), and $a$ and $p$ are free parameters. This relation can be rewritten as an effective $R_V$,

$$R_V = \frac{1}{a(0.8^p - 1)}. \qquad (6)$$

For scattering from LMC (Milky Way) dust, G08 measured $a = 0.9$ ($a = 0.8$) and $p = -1.5$ ($p = -2.5$), respectively, corresponding to $R_V = 1.67$ (2.79).

Circumstellar scattering produces a light echo that is delayed by the light travel time between the SN and the CSM (Wang 2005; Patat et al. 2006; Amanullah & Goobar 2011). For photons arriving at the same time, the light echo and SN SEDs will be different, resulting in temporal differences in spectral features and a changing continuum (Patat et al. 2006; Amanullah & Goobar 2011). The details of how the time-delayed SED contributes to the observed data are not included in our scattering parameterisation (Equation 5).

## 5 PHOTOMETRIC REDDENING ESTIMATES

Spectroscopy provides precise measurements of wavelength-dependent reddening and extinction. Photometry can provide high temporal resolution and potentially probe wavelengths difficult to measure with spectra.

### 5.1 Comparison Supernovae

We presented the SN 2014J light curves in Section 2, and Figure 2 displays those data. In that figure, we compare the SN 2014J light curves to those of SN 2011fe. Below, we also

compare to SNe 2009ig and 2013dy. With the exception of SN 2011iv (Foley et al. 2012b) and SN 2014J, SNe 2011fe and 2013dy are the only SNe Ia with high-quality UV spectral time series from *HST*. Maguire et al. (2012) presented the optical *HST* spectra of SN 2011fe, Foley (2013) presented the maximum-light UV-optical spectrum, and Mazzali et al. (2014) presented the full spectral series. The SN 2013dy spectra will be studied in detail in another publication (Pan et al., in preparation). UV spectra of SN 2009ig were obtained by *Swift* (Foley et al. 2012a). Although these data are not as high quality as the *HST* data, the small number of well-observed SNe Ia with *HST* necessitate their inclusion in this study.

We used SNID (Blondin & Tonry 2007) to determine which SNe were spectrally similar to SN 2014J. SNID removes the continuum from each spectrum, and thus reddening effects are reduced. The overwhelming match for SN 2014J was SN 2007co; spectra of SN 2007co were in the top 5 SNID matches for our 10 *HST* spectra 16 times (32%). Although this is a crude metric that depends on the number of spectra for a given SN at specific epochs in the SNID database, it does indicate that SN 2007co is spectrally similar. Of our comparison SNe with UV spectra, SN 2007co is spectrally most similar to SN 2011fe, and their colour curves have similar evolution, although SN 2007co is about 0.07 mag redder in $B - V$ than SN 2011fe at all epochs.

SN Ia intrinsic colours correlate with both light-curve shape (e.g., Riess et al. 1996) and velocity (Foley & Kasen 2011; Foley 2012; Mandel et al. 2014). It is likely that even for two SNe with exactly the same light-curve shape and velocity, some intrinsic colour scatter exists. In fact, this has been shown for SNe 2011by and 2011fe (Foley & Kirshner 2013). None the less, by comparing SN 2014J to several similar SNe, we hope to probe most of the possible parameter space.

SN 2014J is a somewhat slow decliner ($\Delta m_{15}(B)_{\rm obs} = 0.95$ mag), similar to SNe 2009ig ($\Delta m_{15}(B)_{\rm obs} = 0.89$ mag; Foley et al. 2012a) and 2013dy ($\Delta m_{15}(B)_{\rm obs} = 0.86$ mag; W. Zheng, 2014, private communication). SNe 2007co and 2011fe are slightly faster decliners, with $\Delta m_{15}(B)_{\rm obs} = 1.16$ and 1.10 mag, respectively (e.g., Mandel et al. 2011; Richmond & Smith 2012). However, the measurement of $\Delta m_{15}(B)$ is affected by dust reddening (as the effective wavelength of the filter shifts). Phillips et al. (1999) presented a method to derive a corrected value:

$$\Delta m_{15}(B)_{\rm true} = \Delta m_{15}(B)_{\rm obs} + 0.1 E(B - V). \qquad (7)$$

Below, we argue that $E(B-V) \approx 0.6$–1.3 mag for SN 2014J, which would result in $\Delta m_{15}(B)_{\rm true} = 1.01$–1.08 mag. Similarly, SN 2013dy had moderate reddening, both from its host galaxy and the Milky Way, resulting in $\Delta m_{15}(B)_{\rm true} = 0.89$ mag. SNe 2007co, 2009ig, and 2011fe do not suffer from significant extinction (Mandel et al. 2011; Nugent et al. 2011; Foley et al. 2012a; Johansson et al. 2013; Patat et al. 2013), and the observed decline rate is essentially equivalent to the true decline rate. Therefore, SN 2014J has a decline rate intermediate to SNe 2009ig/2013dy and SNe 2007co/2011fe, but all are similar.

SN 2014J has a relatively high ejecta velocity at maximum brightness. From the $t = -0.4$ day spectrum of SN 2014J, we measure a Si II $\lambda6355$ velocity of $-11{,}870$ km s$^{-1}$. From the $t = -0.4$ day spec-

trum of SN 2013dy, we measure a Si II $\lambda6355$ velocity of $-10{,}370$ km s$^{-1}$. SNe 2007co, 2009ig, and 2011fe have maximum-light Si II $\lambda6355$ velocities of $-12{,}000$ (Foley & Kasen 2011), $-13{,}500$ (Foley et al. 2012c), and $-10{,}400$ km s$^{-1}$ (Foley & Kirshner 2013), respectively. Therefore, SN 2014J has ejecta velocity intermediate to that of SNe 2011fe/2013dy and SN 2009ig, and similar to SN 2007co. Since the intrinsic $B - V$ colours (and presumably flux at shorter wavelengths) of SNe Ia are correlated with ejecta velocity (Foley & Kasen 2011; Foley et al. 2011; Mandel et al. 2014), spanning the range of possible velocities is important.

Although SN 2014J has a longer rise and decline in bluer bands, the redder bands, especially $I$ and $H$, are nearly identical for SNe 2011fe and 2014J (Figure 2). Therefore, a single stretch cannot describe the light-curve differences. Instead, the observed differences in stretch are likely caused by different effective wavelengths (which change with time). Both scattering and dust extinction will affect the bluer bands more, leading to a larger discrepancy in those bands.

Before understanding the reddening for SN 2014J, we must understand (and correct for) the reddening for our comparison SNe. First, we remove all Milky Way reddening as determined by Schlafly & Finkbeiner (2011) using a Fitzpatrick (1999) reddening law and $R_V = 3.1$. For SNe 2007co, 2009ig, and 2011fe, the host-galaxy reddening is estimated to be minimal (e.g., Mandel et al. 2011; Patat et al. 2011; Foley et al. 2012a; Johansson et al. 2013; Phillips et al. 2013)[5]. We make no host-galaxy dust correction for these SNe.

SN 2013dy likely suffers from some host-galaxy dust reddening. Zheng et al. (2013) estimate a reddening of $E(B - V) = 0.15$ mag based on measurements of the Na D lines. However, this method is not particularly accurate (Blondin et al. 2009; Poznanski et al. 2011; Phillips et al. 2013). To account for the possible uncertainty, we deredden SN 2013dy assuming $E(B - V) = 0.15 \pm 0.10$ mag. For SN 2013dy, we use all combinations of reddening, $R_V$ from 1.0 to 3.1, and both F99 and CCM reddening laws; the differences between approaches are included in the overall uncertainty for any results.

## 5.2 Photometric Filters

Knowing the effective wavelength of photometric filters is especially important when inferring reddening properties from photometry. In the UV, the intrinsic flux of a SN Ia decreases to shorter wavelengths, and even a modest amount of reddening can dramatically alter the effective wavelength of some filters. For the WFC3 filters[6], this is compounded by "red leaks," where the transmission of the filters extends (at a low level) far into the optical and NIR.

Figure 6 shows the observed maximum-brightness spectra of SNe 2011fe and 2014J, the transmission curves for the WFC3 filters, and the transmitted spectra of the SNe.

---

[5] Although SN 2009ig appears to have no dust reddening, a light echo has been detected for the SN, indicating that there could be substantial dust along the line of sight to SN 2009ig (Garnavich et al. 2013).
[6] ftp://ftp.stsci.edu/cdbs/comp/wfc3/

We measure the effective wavelength of each filter for both SNe. While the effective wavelengths for the two SNe in F275W and F336W are relatively similar (differing by 70 and 50 Å, respectively), the F218W and F225W filters have significantly different effective wavelengths with differences of 2040 and 960 Å, respectively. As a result of these shifts, these "bluer" filters have an effectively longer wavelength than F275W.

None of the *HST* photometry exclusively probes UV wavelengths for SN 2014J. The effectively bluest filter, F275W, has an effective wavelength of 2960 Å at maximum brightness, but a significant fraction of the photons come from the optical. Since SNe Ia become redder after maximum brightness, the effective wavelengths of the "UV" filters all shift farther to the red. Although these are nominally UV filters, the majority of SN 2014J photons measured through these filters had optical wavelengths. Only our *HST* spectroscopy effectively probes the UV properties of SN 2014J.

There is a significant systematic uncertainty related to the effective wavelength for these filters. More than 50% of the flux for the F218W and F225W filters occurs where the transmission function is <0.1% of the peak transmission. Slight uncertainties in the filter transmission curves at these wavelengths will cause large uncertainties in effective wavelengths *and* any synthetic photometry.

To test the potential systematic uncertainty, we synthesised photometry from our spectra of SN 2014J and compared the results to the photometry. For our optical filters, the synthesised photometry was consistent with the observed photometry to within the photometric uncertainties. However, the UV synthesised photometry was brighter than the observed photometry by roughly 0.15, 0.52, 0.18, and 0.10 mag (the exact amount changes as the spectrum evolves) from the bluest to the reddest bands, respectively. Although our spectra are somewhat noisy at the shortest wavelengths, Figure 6 shows that the majority of the flux in these filters is coming from $\lambda \gtrsim 3000$ Å, where our spectra have a high S/N. These differences are most likely caused by inaccurate filter transmission curves.

The difference in effective wavelength even leads to a systematic uncertainty related to the Milky Way extinction. The difference in the extinction for the nominal and effective wavelength of the F218W filter, for instance, is >0.1 mag for SN 2014J, which has a relatively small Milky Way reddening of $E(B-V) = 0.05$ mag. The exact value for the extinction is extremely uncertain even if one has perfect knowledge of the SED simply because of the uncertainty in the filter transmission.

Because of these systematic effects, the F218W and F225W bands should *never* be used for measuring dust properties of even moderately reddened SNe Ia. The only way to properly probe these UV wavelengths with current instrumentation is with *HST* spectroscopy. For determining the dust and scattering properties for SN 2014J, which is quite reddened, we still use the F275W and F336W photometry, but include systematic uncertainties of 0.18 and 0.10 mag, respectively.

## 5.3 Colour Excess

Since SN 2011fe had essentially no host-galaxy reddening (Nugent et al. 2011; Johansson et al. 2013; Patat et al.
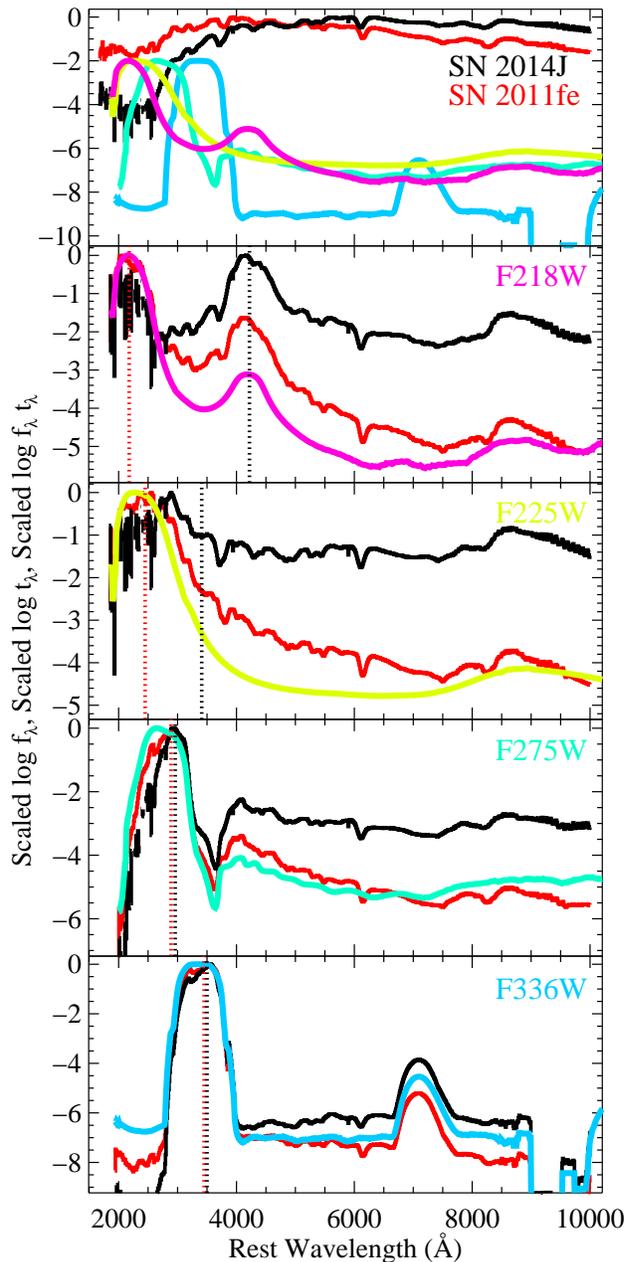


**Figure 6.** (*Top panel*): Maximum-brightness spectra of SNe 2014J (black) and 2011fe (red) scaled such that their peak flux is 1 ($\log f_\lambda = 0$). The magenta, yellow, mint, and light blue curves are the WFC3 F218W, F225W, F275W, and F336W transmission curves, respectively, also scaled such that their peak is 0.01 ($\log t_\lambda = -2$). (*Bottom panels*): From top to bottom, the F218W, F225W, F275W, and F336W transmission curves scaled such that their peak is 1 ($\log t_\lambda = 0$) in the colours labeled above. The solid red and black curves are the transmitted flux (the flux times the transmission curve) for SNe 2011fe and 2014J, respectively, scaled such that their peak is 1 ($\log f_\lambda t_\lambda = 0$). The dotted red and black lines represent the effective wavelength in each filter for SNe 2011fe and 2014J, respectively.

2013), we can approximate $(X - Y)^{\mathrm{obs}}_{11\mathrm{fe}} = (X - Y)^{\mathrm{true}}_{11\mathrm{fe}}$. One can then determine the observed colour excess to SN 2014J by comparing colour curves:

$$E(X - Y)^{\mathrm{obs}}_{14\mathrm{J}} = (X - Y)^{\mathrm{obs}}_{14\mathrm{J}} - (X - Y)_{11\mathrm{fe}}, \qquad (8)$$

where $X$ and $Y$ are any two given photometric bands. This method assumes similar SEDs and spectral evolution.

We use the Richmond & Smith (2012) and Matheson et al. (2012) optical and NIR SN 2011fe light curves. We also synthesise UV light curves from the SN 2011fe UV spectral sequence (Mazzali et al. 2014). For convenience, we provide these synthetic light curves in Table 8.

We interpolate light curves using B-splines. This method, rather than fitting a simple polynomial or a template light curve, is relatively assumption free and provides an excellent description of the data with small residuals. From the interpolated light curves, we derived colour curves and then colour-excess curves. We present the $E(X - V)^{\mathrm{obs}}$ and $E(V - Y)^{\mathrm{obs}}$ colour-excess curves in Figure 7.

Examining Figure 2, the $J$-band light curves for SNe 2011fe and 2014J have different shapes. Since this behaviour is not seen in the $I$ or $H$ bands, we believe this is related to the filter transmission functions for the $J$ band ($S$ corrections; Stritzinger et al. 2002). Matheson et al. (2012) note that their $J$-band light curve of SN 2011fe deviates significantly from template light curves, likely because of the significantly different $J$ filter used for that study. Accordingly, we do not include any $J$-band data in this analysis.

The observed colour excesses for SN 2014J change dramatically with time for some colours. For instance $E(B-V)$, the preferred colour excess to describe the amount of reddening, changes by $\sim$0.4 mag from maximum brightness to one month after maximum brightness. Other colour excesses are quite stable; $E(V - R)$, for example, has a maximum deviation of 0.095 mag and scatter of 0.025 mag from $t = -10$ to $+74$ days. For most colour excesses, there is a measurement error of only a few hundredths of a magnitude.

Since SN Ia SEDs change dramatically with time and heavily reddened (or scattered) SEDs will shift the effective wavelength of a filter, comparisons are necessary to interpret the colour curves and transform $E(X - Y)^{\mathrm{obs}}$ to $E(X - Y)^{\mathrm{true}}$. Observed SN Ia colour-excess curves change with time (e.g., Phillips et al. 1999; Jha et al. 2007), and high-cadence measurements of the observed colour-excess curves are necessary for proper comparison. The Hsiao et al. (2007) template spectra were used for this purpose. These spectra were generated from many different SNe and are close to an "average" spectrum. The high cadence of the template spectra is particularly attractive for comparisons. We also use the *HST* (and NIR when available) spectra of SN 2011fe for validation of the template spectra. It is known that the Hsiao et al. (2007) template spectra do not properly describe the early-time UV behaviour of SNe Ia (Foley et al. 2012a), and the SN 2011fe data should be particularly useful in this regime.

Model colour-excess curves are created by comparing the colour curves of the synthetic photometry of the reddened and/or scattered template and SN 2011fe spectral series relative to the colour curves of the synthetic photometry from the unchanged spectra. If SN 2014J has the same SEDs and temporal evolution as the template spectra, the true reddening parameters will produce colour-excess curves that match those of SN 2014J.

The Tsvetkov et al. (2014) SN 2014J $B - V$ colour curve is $\sim$0.05 mag redder at peak than the one presented here. This is likely caused by $S$ corrections (Stritzinger et al. 2002). Such differences may produce slight shifts (of order 0.05 mag) in the measured colour excess. Because we have multiple bands, and these shifts should be roughly random, the total uncertainty in $E(B - V)$ should be <0.01 mag.

We test the 6 reddening/scattering models listed in Section 4 by reddening/scattering the template spectra and deriving the observed colour excesses. These measurements are compared to the data, and best-fitting parameters for each model are measured. Although our primary comparison is SN 2011fe, we also test how our results vary when using SNe 2009ig and 2013dy, both of which have fewer data than SN 2011fe. All fit parameters have an uncertainty related to the unknown intrinsic colour of SN 2014J, which is $\sim$0.1 mag for $E(B-V)$ and $\sim$0.05 for $R_V$ and $p$. For some model comparisons, this additional uncertainty cancels out, and thus we do not list it below to make more precise comparisons.

The SN 2014J data are inconsistent with the most basic reddening models where $R_V$ is set to 3.1. For the F9931 and CCM31 models, we find best-fitting reddening values of $E(B - V)^{\mathrm{true}} = 0.874 \pm 0.018$ and $0.887 \pm 0.015$ mag with reduced $\chi^2$ of $\chi^2_\nu = 10.4$ and 10.2, respectively. These models result in $A^{\mathrm{true}}_V \approx 2.7$ mag, which is much larger than our observed and model-independent value (Section 3). We do not include the best-fitting colour-excess curves for these models in Figure 7; because of their poor fit, doing so would change the presentation of the figure to the point where one cannot discriminate from other, better-fitting models.

In fact, all simple reddening models with $R_V > 2$ are not good fits to the data. Specifically, $R_V = 2$ yields $\chi^2_\nu = 3.3$ and 2.9 for the F99 and CCM models, respectively.

When allowing $R_V$ to be free, the best-fitting values for the F99 and CCM models are $E(B - V)^{\mathrm{true}} = 1.194 \pm 0.012$ and $1.244 \pm 0.010$ mag with $R^{\mathrm{true}}_V = 1.66 \pm 0.03$ and $1.44 \pm 0.03$, respectively. These models have $\chi^2_\nu = 2.6$ and 1.5, respectively, indicating moderate success at reproducing the observations. At these low values of $R_V$, the derived reddening laws are extrapolations, implying an additional systematic uncertainty not included in this analysis. These models imply $A^{\mathrm{true}}_V = 2.0$ and 1.8 mag, both similar to our model-independent measurements of the extinction: $A^{\mathrm{obs}}_V = 1.95 \pm 0.09$ mag.

The circumstellar material scattering model (CSM) is significantly better at describing the observed data. We find a best-fitting power-law index of $p = -1.977 \pm 0.014$, similar to LMC and Milky Way dust, and $\chi^2_\nu = 0.54$. Fitting the data with a simple power law $(A_\lambda/A_V \propto (\lambda/\lambda_V)^p)$ results in an equally good fit as the G08 model with the same power-law index.

Because of the statistical success of the CSM model, the two-component CSMD model is not strictly necessary. None the less, we test certain physically motivated models and report the results. Fixing $R_V = 3.1$, we find $E(B - V)^{\mathrm{true}} = 0.49 \pm 0.02$ mag and $p = -3.42 \pm 0.15$ with $\chi^2_\nu = 0.55$ — essentially the same as for the best-fitting CSM model. For the Milky Way scattering parameters, we find a worse fit, $E(B - V)^{\mathrm{true}} = 0.796 \pm 0.009$ mag and $R^{\mathrm{true}}_V = 1.40 \pm 0.03$ with $\chi^2_\nu = 1.60$. For the LMC scattering parameters, the
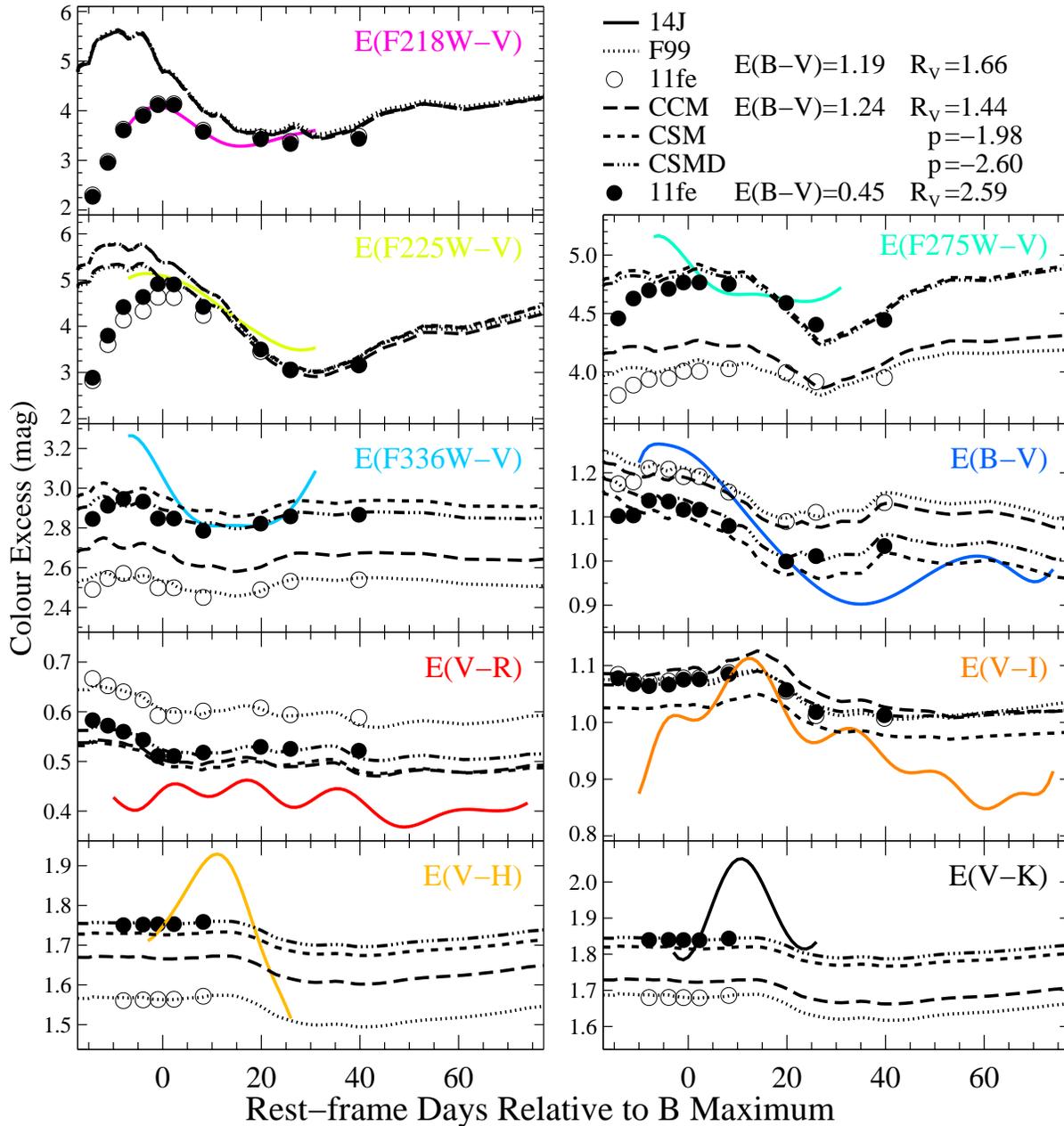
**Figure 7.** Observed colour excesses for SN 2014J (solid curves). Each colour excess is determined from the photometry of SN 2014J relative to that of SN 2011fe, and the plotted colour corresponds to the colour of the non-$V$ band filter used for the colour excess as displayed in Figure 2. Since reddening and scattering change the effective wavelength of each filter and SN SEDs change dramatically with time, the measured colour excess is expected to change in some filters with time. To account for this change, we also present spectrophotometry of template spectra (Hsiao et al. 2007) reddened and/or scattered by various amounts. Four scenarios are shown: F99 reddening with $E(B-V) = 1.19$ mag and $R_V = 1.66$ (dotted curve), CCM reddening with $E(B-V) = 1.24$ and $R_V = 1.44$ (long-dashed curve), CSM scattering with $p = -1.98$ (short-dashed curve), and a combined F99 reddening with $E(B-V) = 0.45$ mag and $R_V = 2.57$ and CSM scattering with $p = -2.57$ (CSMD; dot-dashed curve). The same procedure was done for spectra of SN 2011fe (open circles corresponding to the F99 reddening and filled circles corresponding to the CSMD model).

best-fitting parameters are $E(B-V)^{\rm true} = 0.492 \pm 0.007$ mag and $R_V^{\rm true} = 2.35 \pm 0.05$ with $\chi_\nu^2 = 0.83$. Restricting the scattering power law to $-1.5 \geqslant p \geqslant -2.5$ and $R_V = 3.1$, we find a best-fitting result with $p = -2.5$ and $E(B-V)^{\rm true} = 0.273 \pm 0.008$ mag with $\chi_\nu^2 = 0.58$. Finally, using the best-fitting parameters when fitting to the spectra (Section 6), we measure $\chi_\nu^2 = 0.75$.

There is significant temporal evolution in some colour excesses, which is not matched by the evolution of the best-fitting reddened/scattered templates. Examining the Tsvetkov et al. (2014) colour curves, which have similar shapes to those presented here, this evolution is not the result of $S$ corrections related to the SN 2014J photometry. Alternatively, SN 2014J may have a different colour evolu-

tion than SN 2011fe or the Hsiao et al. (2007) templates. Examining 29 high-quality SN Ia light curves (Hicken et al. 2009a; Contreras et al. 2010) that cover both a week before until a week after maximum brightness, two (7%) have a $B - V$ colour evolution as extreme as that of SN 2014J. The exact reddening parameters have a small effect on the evolution of the comparison colour curves, which in turn affects the amount of variability (at the $\sim$20% level). Because of these different effects, we are not confident that there is temporal evolution of $E(B-V)^{\rm true}$ for SN 2014J.

# 6 SPECTROSCOPIC REDDENING ESTIMATES

One of the best ways to determine the reddening for an astrophysical object is to compare the SEDs of the reddened object to an identical unreddened object. The difference between the measured flux (after correcting for any potential distance difference) at a given wavelength is the extinction for that wavelength. The extinction as a function of wavelength, the extinction curve, can then be compared to the extinction curves expected for different reddening laws.

Here we take a slightly different approach. Instead of assuming the known luminosity of the SN, we only assume that the spectral shapes of SN 2014J and the comparison SNe are similar, leaving the differences in luminosity and distance as a free parameter. Consequently, distance errors do not effect our measurements.

SNe 2009ig, 2011fe, and 2013dy are used as comparison SNe. As mentioned in Section 5.1, these are the three SNe Ia with reasonable UV time series. Table 9 indicates the phase of each SN 2014J spectrum and the comparison spectra of the other SNe.

Spectroscopy provides two particular advantages over photometry. First, because of the reddening, the nominally UV *HST* filters really probe optical wavelengths (Section 5.2) and have uncertain effective wavelengths and Milky Way extinctions. Second, particular spectral features (especially Ca H&K, which is at the blue end of the optical window) even vary significantly between SNe with the same light-curve shape. These features can be excluded from spectral comparisons, but are unavoidable with photometry (unless one completely excludes particular filters).

Because of the effective wavelengths of the photometric filters, our *HST*/STIS spectra are the only proper UV data for SN 2014J.

## 6.1 Method

We tested the 6 models presented in Section 4 by reddening/scattering the SN 2014J spectra to match the phase-matched comparison spectra. First, we fit only UV-optical data (2500–10,000 Å). All SN 2014J and comparison spectra have data over this range. Although the SN 2014J *HST* spectra have data below 2500 Å, the flux is consistent with zero (with large uncertainties). We therefore ignore these data, although they may be important for exotic models. Some comparison spectra also have NIR data; we fit the spectra with and without these data. When fitting the pre- and near-maximum brightness data, we ignore the spectral regions covering Ca H&K, the Ca NIR triplet, and the Si II
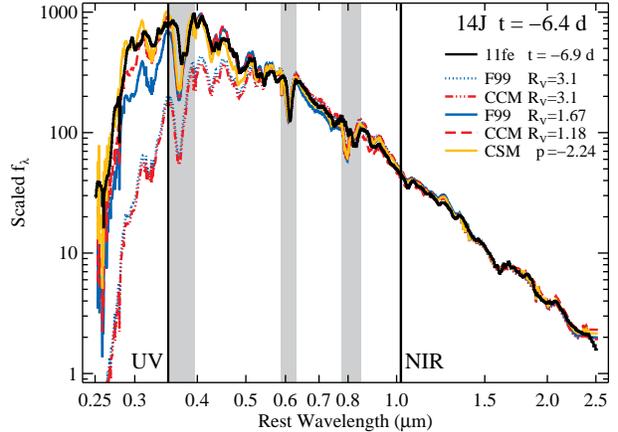


**Figure 8.** UVOIR $t = -6.4$ day spectrum of SN 2014J dereddened or descattered by the best-fitting reddening (F9931, CCM31, F99, and CCM) and circumstellar scattering (CSM) curves to match the $t = -6.9$ day SN 2011fe spectrum (black curve). We do not plot the best-fitting two-component circumstellar scattering and reddening model (CSMD) since it is very similar to the best-fitting CSM model (despite having different parameters). The regions excluded from the fitting, corresponding to Ca H&K, Si II $\lambda$6355, and the Ca NIR triplet, have been marked by the grey regions. The UV and NIR regions are noted. Most of the discriminating power comes from the UV, which is not probed by the photometry, but the NIR is helpful in anchoring the models.

$\lambda$6355 feature. Differences in line depths and velocity can significantly affect the flux at these wavelengths in ways that are unrelated to dust reddening.

For presentation purposes, we generally plot the pseudo-extinction curve,

$$X_\lambda/X_V = \frac{f_\lambda^{\rm SN}/f_\lambda^{\rm 14J}}{f_\lambda^{\rm SN}(5500\ {\rm Å})/f_\lambda^{\rm 14J}(5500\ {\rm Å})}, \qquad (9)$$

where $f_\lambda^{\rm 14J}$ and $f_\lambda^{\rm SN}$ are the flux of SN 2014J and the comparison SN, respectively. This function is scaled by the flux ratios at the $V$ band (roughly 5500 Å). This curve is not an extinction curve since the normalisation is arbitrary to compensate for the uncertainty in the SN luminosities and distances. Reddening curves can then be directly compared. When comparing two sets of data or models to the data, we can then use the residuals to determine $\Delta A_\lambda$ and still avoid distance/luminosity uncertainties.

## 6.2 Single-Component Reddening Models

We first examine the single-component reddening models: CCM31, F9931, CCM, and F99. These models require a single value for $E(B-V)^{\rm true}$ and $R_V^{\rm true}$ for each spectral pair and are the most simplistic reddening models of our tested possibilities.

The $t = -6.4$ day spectrum of SN 2014J, dereddened by the best-fitting extinction curves, is displayed in Figure 8. This figure represents the output of the spectral matching.

Figures 9 and 10 show the pseudo-extinction curves for the $t = -6.4$ day SN 2014J spectrum (compared to the $t = -6.9$ day SN 2011fe and $t = -6.2$ day SN 2013dy spec-
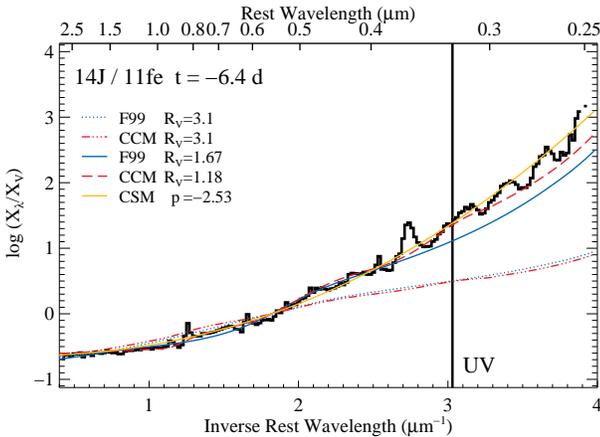
**Figure 9.** Pseudo-extinction curve of SN 2014J at $t = -6.4$ days determined by comparing to SN 2011fe (black curve). Various reddening curves and scattering models corresponding to those presented in Figure 8 are overplotted. The data are incompatible with an $R_V = 3.1$ reddening law.
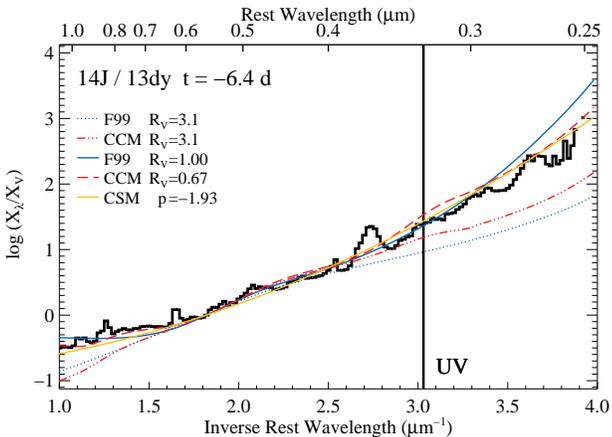


**Figure 10.** Same as Figure 9, but using SN 2013dy as the comparison and with slightly different model parameters.

tra, respectively). Overplotted are the best-fitting extinction curves for the above scenarios.

The most obvious result of the above analysis is that the SN 2014J spectra are inconsistent with simple reddening with $R_V = 3.1$, similar to what was determined from the photometry (Section 5.3). Such reddening laws consistently undercorrect the UV.

When $R_V$ is allowed to vary, the data are reasonably fit with a single reddening law; however, extremely low values for $R_V$ are required. For instance, using the CCM law and comparing to SN 2013dy, the highest best-fitting value for any spectral pair is $R_V = 2.0$.

The best-fitting values for the CCM and F99 models change dramatically with time. Figure 11 displays the best-fitting CCM values of $E(B - V)^{\rm true}$ and $R_V^{\rm true}$ for SN 2014J as a function of time. Each SN 2014J spectrum is fit separately. All epochs are consistent with $E(B - V)^{\rm true} = 1.49 \pm 0.09$ mag, but $R_V^{\rm true}$ increases from 0.67 to 1.89 over the span of one month. The UV portion of our spectra is not
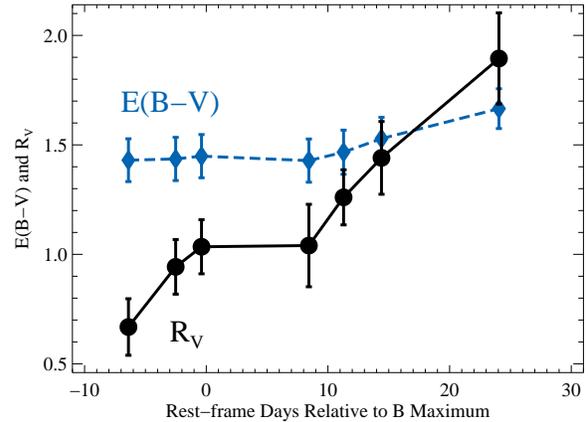


**Figure 11.** Measurements of $E(B - V)^{\rm true}$ (blue diamonds) and $R_V^{\rm true}$ (black circles) for SN 2014J as a function of time. The measurements are made by comparing spectra of SN 2014J to those of SN 2013dy at similar phases. We assume a CCM reddening law, and SN 2013dy has been dereddened by $E(B-V)_{\rm host} = 0.15$ mag. The uncertainties are dominated by the uncertainty in the host-galaxy reddening of SN 2013dy.

the cause of this change; using only data with $\lambda > 3000$ Å, we find a mean reddening of $E(B - V)^{\rm true} = 1.55 \pm 0.10$ mag and $R_V^{\rm true}$ increasing from 0.76 to 1.65. The photometry of SN 2014J showed similar behaviour with $E(B - V)^{\rm obs}$, although we were not confident that the photometric derivation of $E(B - V)^{\rm obs}$ was truly varying.

No physical model of dust formation/destruction or different clouds of dust entering/exiting the SN beam can have unchanging reddening and changing $R_V$. It is possible that dust grains coagulate to form larger grains on average, but it is unlikely that this process would occur on these timescales. Therefore, these simple reddening models cannot explain the SN 2014J observations.

Many of the best-fitting values for $R_V$ are unphysically low. The expectation for Rayleigh scattering is $R_V \approx 1.2$, with smaller values being extremely unlikely. This alone may indicate a problem with a pure reddening scenario; however, the reddening laws are extrapolations for these values of $R_V$, and thus the true value of $R_V$ may be larger than what is measured.

### 6.3 Circumstellar Scattering

Using the CSM scattering model described in Section 4, we can correct the SN 2014J spectra to be roughly consistent with the spectra of the other SNe. However, circumstellar scattering does not provide a better fit than the reddening laws (over all spectra).

Similar to the dust reddening parameters, the circumstellar scattering parameters change with epoch. For instance, the power-law exponent, $p$, changes from $-2.1$ to $-1.4$ when comparing to SN 2013dy. Although this is potentially physically possible if dust were being actively destroyed, revealing a different grain-size distribution, no specific prediction has been made.
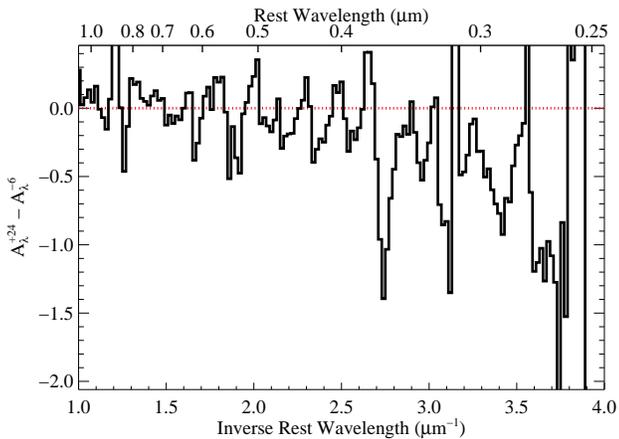
**Figure 12.** Difference in the extinction curves for SN 2014J at $t = -6$ and $+24$ days as determined by comparing to SN 2011fe spectra at similar epochs.

## 6.4 Variable Extinction?

Given that the best-fitting parameters change as SN 2014J evolves with time, we wish to determine if the changing parameters are caused by physical differences or poor fitting. Using SN 2011fe as an intermediary, we compare the extinction curves of SN 2014J at $t = -6.4$ days and $t = +24.1$ days in Figure 12. For the two epochs, the extinction is similar in the optical, but differs significantly in the UV with the $t = -6.4$ day extinction curve having significantly more extinction in the UV.

Either the extinction curves are changing with time or SN 2014J has significantly different colour evolution than SN 2011fe. SN 2014J is spectrally most similar to SN 2007co, which has a similar colour evolution to SN 2011fe, but is redder for all epochs. Therefore, SN 2011fe should be a good comparison for this task, although the exact extinction difference at a given wavelength may be slightly different if SN 2007co were used[7].

Patat et al. (2006) showed that for circumstellar dust the inferred extinction curve, when comparing spectral pairs, should change dramatically from maximum until at least one month after maximum brightness. The derived curves should be roughly the same in the red for both epochs, but in the blue, the later spectral comparison should indicate a decrease in $A_\lambda$ relative to what was measured at maximum brightness. SN 2014J displays this behaviour in Figure 12.

## 6.5 Multiple-Component Extinction

Given the deficiencies in single-component models describing the extinction toward SN 2014J, we turn to the CSMD model. Given the complexity of M82 and the fact that SN 2014J is in its disc, there is likely ISM dust in addition to any possible circumstellar dust or scattering.

Adding a dust component to the circumstellar scattering model, CSMD, resulted in two components of roughly

---

[7] Unfortunately, there are no existing UV spectra of SN 2007co, and thus a comparison at the most interesting wavelengths cannot be made.
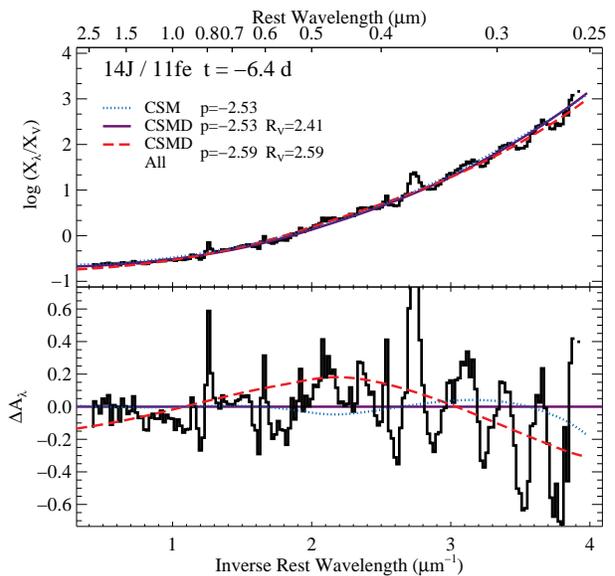


**Figure 13.** (*Top panel*): Pseudo-extinction curve of SN 2014J at $t = -6.4$ days determined by comparing to SN 2011fe (black curve). Various reddening curves and scattering models are overplotted. Similar to Figure 9. (*Bottom panel*): Residual extinction of SN 2014J at $t = -6.4$ days relative to the best-fitting two-component dust reddening and circumstellar scattering model. Also shown are the residual extinction of two-component dust reddening and circumstellar scattering models with best-fitting parameters for the full spectral time series (dashed red curve) and the circumstellar scattering only model for this epoch (dotted blue curve).

equal weight. These models have best-fitting $E(B - V) \approx 0.6$ mag, roughly half that of the single-component models. Intriguingly, $R_V$ also generally increased. Meanwhile, the parameters for the scatter component were $a \approx 0.6$ and $p \approx -2.7$, roughly consistent with the LMC dust model of G08 and similar to good fits to the photometry (Section 5.3). However, we caution that there are some degeneracies between these components, and the solutions are not particularly well determined for any specific spectral pair. To compensate for these degeneracies, we also fit the entire time series at once.

The pseudo-extinction curves for SN 2014J at $t = -6.4$ and 24.1 days are presented in Figures 13 and 14, respectively. They are compared to the best-fitting CSM and CSMD models for each individual epoch and the best-fitting CSMD model for all epochs. For these two examples, the various models do not vary significantly.

While the single set of best-fitting parameters for all spectra does not provide the best fit for any individual spectrum (as one would expect), the $\chi_\nu^2$ for each spectrum does not dramatically increase. The best-fitting values for this case (when comparing to SN 2011fe) are $E(B - V)^{\mathrm{true}} = 0.45 \pm 0.02$ mag, $R_V^{\mathrm{true}} = 2.59 \pm 0.02$, $a = 0.83 \pm 0.05$, and $p = -2.60 \pm 0.06$ for a F99 reddening law. These values represent a reasonable amount of dust reddening with typical properties and circumstellar scattering off LMC-like dust.

We also show the CSMD colour-excess curves for these parameters in Figure 7. This model is a good fit to the photometric data in addition to the spectral data.
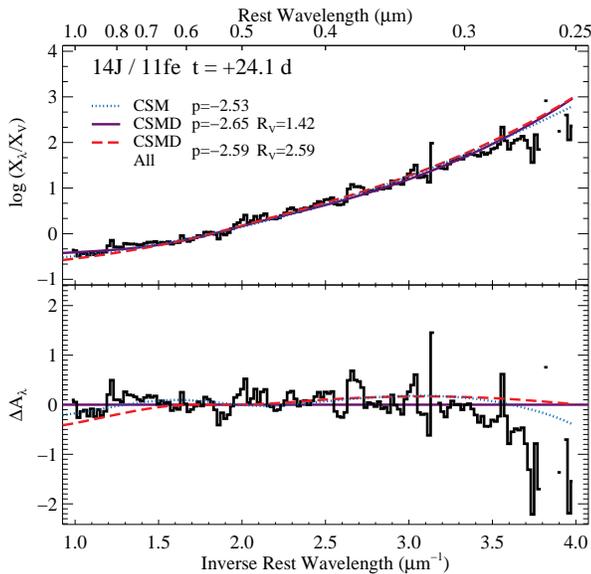
**Figure 14.** Same as Figure 13, but for the $t = 24.1$ day spectrum of SN 2014J.

We present our SN 2014J *HST* spectra, dereddened and descattered by the globally best-fitting CSMD parameters, in Figure 15. The spectra are compared to the Hsiao et al. (2007) template spectra at similar epochs. Overall there is good agreement, especially considering that the parameters are not the result of fitting to the template spectra.

### 6.6 Model Comparison

The SN 2014J spectroscopy is inconsistent with pure reddening laws with $R_V > 2$. The three reasonable models based on spectral comparisons alone are a dust-reddening law with $R_V < 2$, the CSM model, and the hybrid CSMD model.

Allowing reddening parameters to vary for each spectral pair, we find a total (over all spectra) $\chi_\nu^2 = 37.1$, 27.6, and 23.2 for the F99, CSM, and CSMD models, respectively. These relatively large values result from spectral features causing the SN 2014J reddening law to deviate from smooth curves; relative comparisons are still indicative of the quality of fitting. The CSM and CSMD models perform better than the F99 model. Since the F99 model is an extrapolation to $R_V < 2$, the poor fitting may be the result of this extrapolation.

Forcing all epochs to have the same reddening parameters, we find a total $\chi_\nu^2 = 72.1$, 53.4, and 50.3 for the F99, CSM, and CSMD models, respectively. The larger $\chi_\nu^2$ values are caused by the changing continuum with time, which cannot be accounted for by fixing parameters for all epochs. All $\chi_\nu^2$ values doubled by fixing these parameters. Again, the CSM and CSMD models perform better than the F99 model.

## 7 DISCUSSION & CONCLUSIONS

We presented 10 *HST*/STIS spectra of SN 2014J from $-6.4$ to $+24.1$ days relative to *B*-band maximum brightness. We
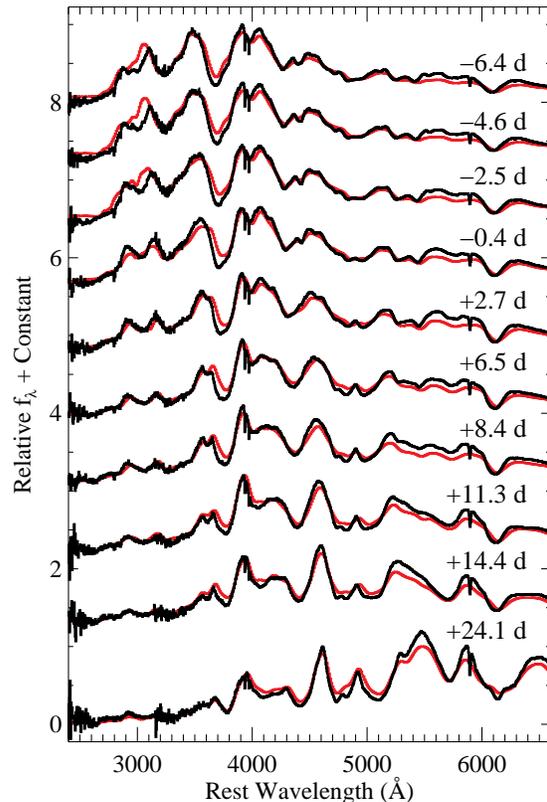


**Figure 15.** Our full *HST* spectral series of SN 2014J (black curves) dereddened by a F99 reddening law with $E(B-V) = 0.45$ mag and $R_V = 2.57$, and descattered by a G08 circumstellar scattering model with $a = 0.84$ and $p = -2.59$ (the globally best-fitting parameters for the CSMD model). Template spectra (Hsiao et al. 2007) at similar epochs are shown in red. The pre-maximum brightness template spectra are known to be inaccurate at UV wavelengths.

supplemented these UV-optical spectra with several NIR spectra of SN 2014J. We also present 17-band photometry from *HST*/WFC3, KAIT, and FanCam. Because of red leaks in the WFC3 UV filters, our photometry does not effectively probe the UV SED of SN 2014J. This extensive dataset is one of the best for a SN Ia in terms of temporal and wavelength sampling.

There is significant extinction toward SN 2014J. Previous studies have applied inaccurate Milky Way reddening corrections to SN 2014J, which have biased measurements of the SN 2014J extinction arising in M82. Using model-independent methods, we determine that extinction to be $A_V^{obs} = 1.95 \pm 0.09$ mag and the reddening to be $E(B-V)^{obs} = 1.19 \pm 0.14$ mag. Comparing these values, we find $R_V^{obs} = 1.64 \pm 0.16$.

Because of the complex dust structures in M82 and the position of SN 2014J within M82, it is extremely likely that there is some interstellar dust reddening in M82. SN 2014J is offset by a projected distance of 1.0 kpc from the nucleus of M82, located in the disc (Figure 1). Hutton et al. (2014) examined the dust properties of M82, finding a luminosity-weighted reddening of $E(B-V) \approx 0.5$ mag for a projected distance of 1 kpc with $R_V \approx 3.1$.

Strong DIB absorption in high-resolution spectra of SN 2014J also indicates that there is a relatively large amount of dust reddening. For the 5780 Å DIB feature, we measured an equivalent width of $344 \pm 21$ mÅ (including a Milky Way contribution which should be $\lesssim 5\%$ of the total). This value is consistent with that found by Welty et al. (2014), but highly inconsistent with that of Goobar et al. (2014). The DIB measurement implies $A_V = 1.8 \pm 0.9$ mag (or $A_V = 2.5 \pm 1.3$ mag for the Goobar et al. 2014 measurement).

Examining the colour excesses in multiple bands and the UV through NIR spectra, which do not depend on the distance to M82, we determine that dust with $R_V = 3.1$, the canonical value for the Milky Way, cannot be the exclusive source of reddening for SN 2014J. In fact, we place a strong constraint of $R_V < 2$ for single-component dust reddening.

From our measured colour excesses, the best-fitting parameters for the F99 and CCM models are $E(B-V)^{\mathrm{true}} = 1.19 \pm 0.10$ and $1.24 \pm 0.10$ mag with $R_V = 1.66 \pm 0.06$ and $1.44 \pm 0.06$ (including systematic uncertainties), respectively, from the photometry. Reddening the maximum-brightness SN 2011fe spectrum by these values, we measure $A_V^{\mathrm{obs}} = 1.91$ mag (1.82 mag) and $E(B-V)^{\mathrm{obs}} = 1.19$ mag (1.17 mag) for the F99 (CCM) model, consistent with the model-independent measurements.

The best-fitting $R_V$ for SN 2014J is consistent with those of other highly reddened SNe Ia (e.g., Elias-Rosa et al. 2006, 2008; Krisciunas et al. 2006; Wang et al. 2008), but are inconsistent with essentially all local lines of sight in the Milky Way (e.g., Fitzpatrick & Massa 2007). The extinction measured from the spectroscopy varies with epoch, which is difficult to explain with only ISM dust reddening. Using a model-independent approach, we see that the extinction at shorter wavelengths increases with time. Because of the variations seen in the spectra, systematic effects related to the effective wavelength of the photometric filters or differing spectral features between SN 2014J and comparison SNe are not the cause of the variation.

Using the same *HST* photometric data presented here (although independently reduced) combined with independent optical and NIR photometry, Amanullah et al. (2014) examined the reddening toward SN 2014J, concluding that $R_V \lesssim 2$ for dust-reddening scenarios. Amanullah et al. (2014) suggest best-fitting parameters of $E(B-V)^{\mathrm{true}} = 1.37 \pm 0.03$ and $R_V^{\mathrm{true}} = 1.4 \pm 0.1$ for a F99 reddening law. Goobar et al. (2014) used the Schlafly & Finkbeiner (2011) catalogue value of $E(B-V) = 0.14$ mag for the Milky Way reddening. Amanullah et al. (2014) used the raw Dalcanton et al. (2009) value of $E(B-V) = 0.06$ mag for the Milky Way reddening, but this value is on the Schlegel et al. (1998) scale. We use the Dalcanton et al. (2009) value on the Schlafly & Finkbeiner (2011) scale: $E(B-V) = 0.05$ mag. Adjusting the Amanullah et al. (2014) reddening value to account for the correct Milky Way extinction results in $E(B-V)^{\mathrm{true}} = 1.38$ mag. This value is larger than our best-fitting value, but is consistent. Reddening the maximum-brightness SN 2011fe spectrum by the corrected values, we measure $A_V^{\mathrm{obs}} = 1.84$ mag and $E(B-V)^{\mathrm{obs}} = 1.39$ mag for a F99 reddening law, which are consistent with the model-independent measurements.

A relatively simple circumstellar scattering model (G08) can reproduce the reddening of SN 2014J. The best-fitting CSM model for our photometry has $p = -1.98 \pm 0.05$, consistent with the Amanullah et al. (2014) value of $p = -2.1 \pm 0.1$.

Variable extinction and colour excess is predicted in circumstellar matter scattering models (Wang 2005; Patat et al. 2006). The G08 model does not attempt to model the temporal variability that must be introduced through the scattering process. None the less, some specific predictions of Patat et al. (2006) are well matched by SN 2014J.

From about a week before maximum brightness until about a month after, narrow ISM and/or CSM absorption features in the spectra of SN 2014J do not vary. Previous detections of variability have been interpreted as evidence for CSM (Patat et al. 2007; Blondin et al. 2009; Simon et al. 2009). A lack of variability may constrain the mass and distance to any potential CSM. Our current observations cannot rule out the existence of CSM, but are consistent with all absorbing gas being purely interstellar.

Given the position of SN 2014J in M82 and the strong DIB absorption, it is incredibly unlikely that there is *no* interstellar dust reddening for SN 2014J. Therefore, the CSM model is unlikely from this simple argument. The extreme values for $R_V$ and the variable extinction also argue against a simple dust-reddening model. Although neither model is ruled out by our data, a promising model is a combination of the two.

Fitting a two-component circumstellar scattering and dust reddening model to the data, we find a consistent picture. The reddening of SN 2014J is well reproduced by a reasonable amount of reddening ($E(B-V) = 0.45$ mag) from relatively typical dust ($R_V = 2.59$) with circumstellar dust parameters similar to those for LMC-like dust. These values represent the best measurements of the dust and reddening properties for SN 2014J. In this scenario, roughly half of the extinction is caused by dust reddening ($A_V = 1.17$ mag) and the other half from scattering. The dust-reddening parameters for this model are remarkably similar to the estimates of the reddening based on the position of SN 2014J (Hutton et al. 2014). They are also consistent with the implied reddening from the high-resolution spectroscopy. Finally, circumstellar scattering predicts a change in the measured extinction at bluer wavelengths with time, consistent with our observations.

It is unlikely that SN 2014J is the only SN Ia with both dust reddening and circumstellar scattering. Re-examination of SNe Ia with high reddening and measurements of a low $R_V$ may reveal similar configurations for these SNe as well. The best-fitting value of $R_V$ for SN 2014J is 2.59, similar to many lines of sight in the Milky Way and similar to that found for low-reddening SNe Ia (when properly accounting for intrinsic colour). Therefore, a CSMD model may solve the problem of small measured values of $R_V$ for high-reddening SNe Ia.

The *HST* UV spectra are very constraining for the reddening models. Thankfully, SNe 2011fe and 2013dy had 10 epochs of spectroscopy each, allowing for several comparisons of spectra with similar phases. Additional SNe Ia with UV spectroscopy will further improve constraints for SN 2014J and future events.

More detailed modelling of how circumstellar scattering affects the SED with time may be the best way to con-

strain CSM parameters using SN SEDs. However, more direct methods such as observations of the circumstellar gas in absorption (e.g., Patat et al. 2007; Sternberg et al. 2011; Foley et al. 2012c; Maguire et al. 2013) and radio/X-ray observations (e.g., Chomiuk et al. 2012; Horesh et al. 2012; Margutti et al. 2012, 2014) may provide the best understanding of the circumstellar environments of SNe Ia.

Being the closest detected SN Ia in at least 28 years, and perhaps in 410 years, SN 2014J will be an important event for understanding SN Ia physics for decades. Here, we have begun to unravel the reddening, a key component in further understanding of the event. A proper measurement of the dust reddening will be especially important for multi-wavelength studies and the long-term monitoring of SN 2014J.

## REFERENCES

Amanullah R., Goobar A., 2011, ApJ, 735, 20
Amanullah R. et al., 2014, ApJ, 788, L21
Ayani K., 2014, Central Bureau Electronic Telegrams, 3792, 1
Betoule M. et al., 2014, ArXiv e-prints
Blondin S., Prieto J. L., Patat F., Challis P., Hicken M., Kirshner R. P., Matheson T., Modjaz M., 2009, ApJ, 693, 207
Blondin S., Tonry J. L., 2007, ApJ, 666, 1024
Burns C. R. et al., 2011, AJ, 141, 19
Cao Y., Kasliwal M. M., McKay A., Bradley A., 2014, The Astronomer's Telegram, 5786, 1
Cardelli J. A., Clayton G. C., Mathis J. S., 1989, ApJ, 345, 245
Chandler C. J., Marvil J., 2014, The Astronomer's Telegram, 5812, 1
Chandra P., Basu A., Ray A., Chakraborty S., 2014, The Astronomer's Telegram, 5804, 1
Chomiuk L. et al., 2012, ApJ, 750, 164
Chomiuk L., Zauderer B. A., Margutti R., Soderberg A., 2014, The Astronomer's Telegram, 5800, 1
Contreras C. et al., 2010, AJ, 139, 519
Cushing M. C., Vacca W. D., Rayner J. T., 2004, PASP, 116, 362
Dalcanton J. J. et al., 2009, ApJS, 183, 67
Denisenko D. et al., 2014, The Astronomer's Telegram, 5795, 1
Dhungana G., Silverman J. M., Vinko J., Wheeler J. C., Marion G. H., Kehoe R., Ferrante F. V., 2014, Central Bureau Electronic Telegrams, 3792, 1
Elias-Rosa N. et al., 2006, MNRAS, 369, 1880
Elias-Rosa N. et al., 2008, MNRAS, 384, 107
Filippenko A. V., Li W. D., Treffers R. R., Modjaz M., 2001, in ASP Conf. Ser. 246: IAU Colloq. 183: Small Telescope Astronomy on Global Scales, Paczynski B., Chen W.-P., Lemme C., eds., pp. 121–+
Fitzpatrick E. L., 1999, PASP, 111, 63
Fitzpatrick E. L., Massa D., 2007, ApJ, 663, 320
Folatelli G. et al., 2010, AJ, 139, 120
Foley R. J., 2012, ApJ, 748, 127
Foley R. J., 2013, MNRAS, 435, 273

Foley R. J., 2014, The Astronomer's Telegram, 5811, 1

Foley R. J. et al., 2012a, ApJ, 744, 38

Foley R. J., Kasen D., 2011, ApJ, 729, 55

Foley R. J., Kirshner R. P., 2013, ApJ, 769, L1

Foley R. J. et al., 2012b, ApJ, 753, L5

Foley R. J., Sanders N. E., Kirshner R. P., 2011, ApJ, 742, 89

Foley R. J. et al., 2012c, ApJ, 752, 101

Fossey J., Cooke B., Pollack G., Wilde M., Wright T., 2014, Central Bureau Electronic Telegrams, 3792, 1

Füresz G., 2008, PhD thesis, Univ. of Szeged, Hungary

Ganeshalingam M. et al., 2010, ApJS, 190, 418

Garnavich P. M., Milne P., Bryngelson G. L., Leising M. D., 2013, in American Astronomical Society Meeting Abstracts, Vol. 222, American Astronomical Society Meeting Abstracts, p. 209.04

Gerke J. R., Kochanek C. S., Prieto J. L., Stanek K. Z., Macri L. M., 2011, ApJ, 743, 176

Gerke J. R., Kochanek C. S., Stanek K. Z., 2014, The Astronomer's Telegram, 5808, 1

Goobar A., 2008, ApJ, 686, L103

Goobar A. et al., 2014, ApJ, 784, L12

Guy J., Astier P., Nobili S., Regnault N., Pain R., 2005, A&A, 443, 781

Hicken M. et al., 2009a, ApJ, 700, 331

Hicken M., Wood-Vasey W. M., Blondin S., Challis P., Jha S., Kelly P. L., Rest A., Kirshner R. P., 2009b, ApJ, 700, 1097

Horesh A. et al., 2012, ApJ, 746, 21

Hsiao E. Y., Conley A., Howell D. A., Sullivan M., Pritchet C. J., Carlberg R. G., Nugent P. E., Phillips M. M., 2007, ApJ, 663, 1187

Hutton S., Ferreras I., Wu K., Kuin P., Breeveld A., Yershov V., Cropper M., Page M., 2014, MNRAS, 440, 150

Itoh R., Takaki K., Ui T., Kawabata K. S., M. Y., 2014, Central Bureau Electronic Telegrams, 3792, 1

Jha S., Riess A. G., Kirshner R. P., 2007, ApJ, 659, 122

Johansson J., Amanullah R., Goobar A., 2013, MNRAS, 431, L43

Kanneganti S., Park C., Skrutskie M. F., Wilson J. C., Nelson M. J., Smith A. W., Lam C. R., 2009, PASP, 121, 885

Kattner S. et al., 2012, PASP, 124, 114

Kelly P. L. et al., 2014, ArXiv e-prints

Krisciunas K., Phillips M. M., Suntzeff N. B., 2004, ApJ, 602, L81

Krisciunas K., Prieto J. L., Garnavich P. M., Riley J.-L. G., Rest A., Stubbs C., McMillan R., 2006, AJ, 131, 1639

Krist J. E., Hook R. N., Stoehr F., 2011, in Society of Photo-Optical Instrumentation Engineers (SPIE) Conference Series, Vol. 8127, Society of Photo-Optical Instrumentation Engineers (SPIE) Conference Series

Ma B., Wei P., Shang Z., Wang L., Wang X., 2014, The Astronomer's Telegram, 5794, 1

Maguire K. et al., 2012, MNRAS, 426, 2359

Maguire K. et al., 2013, MNRAS, 436, 222

Maksym W. P., Irwin J. A., Keel W. C., Burke D., Schawinski K., 2014, The Astronomer's Telegram, 5798, 1

Mandel K. S., Foley R. J., Kirshner R. P., 2014, ArXiv e-prints

Mandel K. S., Narayan G., Kirshner R. P., 2011, ApJ, 731, 120

Mandel K. S., Wood-Vasey W. M., Friedman A. S., Kirshner R. P., 2009, ApJ, 704, 629

Margutti R., Parrent J., Kamble A., Soderberg A. M., Foley R. J., Milisavljevic D., Drout M. R., Kirshner R., 2014, ArXiv e-prints

Margutti R. et al., 2012, ApJ, 751, 134

Marion G. H. et al., 2014, ArXiv e-prints

Matheson T. et al., 2012, ApJ, 754, 19

Mazzali P. A. et al., 2014, MNRAS, 439, 1959

Nielsen M. T. B., Gilfanov M., Woods T. E., Nelemans G., 2014, The Astronomer's Telegram, 5799, 1

Nobili S. et al., 2005, A&A, 437, 789

Nugent P., Kim A., Perlmutter S., 2002, PASP, 114, 803

Nugent P. E. et al., 2011, Nature, 480, 344

O'Donnell J. E., 1994, ApJ, 422, 158

Patat F., Benetti S., Cappellaro E., Turatto M., 2006, MNRAS, 369, 1949

Patat F. et al., 2007, Science, 317, 924

Patat F., Chugai N. N., Podsiadlowski P., Mason E., Melo C., Pasquini L., 2011, A&A, 530, A63

Patat F. et al., 2013, A&A, 549, A62

Patat F. et al., 2014, The Astronomer's Telegram, 5830, 1

Perlmutter S. et al., 1999, ApJ, 517, 565

Phillips M. M., Lira P., Suntzeff N. B., Schommer R. A., Hamuy M., Maza J., 1999, AJ, 118, 1766

Phillips M. M. et al., 2013, ApJ, 779, 38

Poznanski D., Ganeshalingam M., Silverman J. M., Filippenko A. V., 2011, MNRAS, 415, L81

Prieto J. L., Rest A., Suntzeff N. B., 2006, ApJ, 647, 501

Rayner J. T., Toomey D. W., Onaka P. M., Denault A. J., Stahlberger W. E., Vacca W. D., Cushing M. C., Wang S., 2003, PASP, 115, 362

Rest A. et al., 2013, ArXiv e-prints

Richmond M. W., Smith H. A., 2012, Journal of the American Association of Variable Star Observers (JAAVSO), 40, 872

Riess A. G. et al., 1998, AJ, 116, 1009

Riess A. G., Press W. H., Kirshner R. P., 1996, ApJ, 473, 88

Schlafly E. F., Finkbeiner D. P., 2011, ApJ, 737, 103

Schlegel D. J., Finkbeiner D. P., Davis M., 1998, ApJ, 500, 525

Scolnic D. et al., 2013, ArXiv e-prints

Scolnic D. M., Riess A. G., Foley R. J., Rest A., Rodney S. A., Brout D. J., Jones D. O., 2014, ApJ, 780, 37

Simon J. D. et al., 2009, ApJ, 702, 1157

Skrutskie M. F. et al., 2006, AJ, 131, 1163

Sternberg A. et al., 2011, Science, 333, 856

Stetson P. B., 1987, PASP, 99, 191

Stritzinger M. et al., 2002, AJ, 124, 2100

Tsvetkov D. Y., Metlov V. G., Shugarov S. Y., Tarasova T. N., Pavlyuk N. N., 2014, ArXiv e-prints

Tully R. B., 1988, Nearby galaxies catalog

Vacca W. D., Cushing M. C., Rayner J. T., 2003, PASP, 115, 389

Wang L., 2005, ApJ, 635, L33

Wang X. et al., 2009, ApJ, 699, L139

Wang X. et al., 2008, ApJ, 675, 626

Welty D. E., Ritchey A. M., Dahlstrom J. A., York D. G., 2014, ArXiv e-prints

Wood-Vasey W. M. et al., 2008, ApJ, 689, 377

Yun M. S., Ho P. T. P., Lo K. Y., 1994, Nature, 372, 530

Table 1.   *HST* Photometry

| MJD | Filter | Magnitude |
|---|---|---|
| 56685.119 | F218W | 18.158 (021) |
| 56688.845 | F218W | 18.020 (019) |
| 56692.160 | F218W | 18.082 (017) |
| 56696.859 | F218W | 18.309 (023) |
| 56702.568 | F218W | 18.861 (019) |
| 56712.989 | F218W | 19.767 (038) |
| 56723.031 | F218W | 20.505 (043) |
| 56685.122 | F225W | 18.637 (019) |
| 56688.847 | F225W | 18.498 (017) |
| 56692.162 | F225W | 18.619 (019) |
| 56696.862 | F225W | 18.946 (020) |
| 56702.571 | F225W | 19.304 (021) |
| 56712.991 | F225W | 19.541 (025) |
| 56723.034 | F225W | 19.737 (017) |
| 56685.124 | F275W | 16.550 (015) |
| 56688.849 | F275W | 16.440 (014) |
| 56692.164 | F275W | 16.743 (017) |
| 56696.864 | F275W | 17.291 (018) |
| 56702.573 | F275W | 18.086 (021) |
| 56712.993 | F275W | 19.188 (031) |
| 56723.037 | F275W | 19.747 (020) |
| 56685.125 | F336W | 13.096 (008) |
| 56688.850 | F336W | 13.037 (008) |
| 56692.166 | F336W | 13.359 (009) |
| 56696.865 | F336W | 13.843 (012) |
| 56702.574 | F336W | 14.702 (006) |
| 56712.995 | F336W | 16.048 (010) |
| 56723.039 | F336W | 16.824 (010) |
| 56688.892 | F438W | 11.876 (004) |
| 56696.888 | F438W | 12.228 (003) |
| 56702.596 | F438W | 12.629 (006) |
| 56713.017 | F438W | 13.807 (010) |
| 56685.147 | F467M | 11.808 (007) |
| 56692.225 | F467M | 11.649 (004) |
| 56688.893 | F555W | 10.817 (002) |
| 56696.889 | F555W | 11.069 (001) |
| 56702.598 | F555W | 11.278 (002) |
| 56713.018 | F555W | 11.778 (003) |
| 56685.149 | F631N | 10.036 (008) |
| 56692.227 | F631N | 9.940 (005) |
| 56688.894 | F814W | 9.799 (002) |
| 56696.891 | F814W | 10.131 (001) |
| 56702.599 | F814W | 10.357 (002) |
| 56713.019 | F814W | 10.196 (002) |
| 56685.150 | F845M | 9.639 (003) |
| 56692.228 | F845M | 9.664 (002) |

Zheng W. et al., 2014, ApJ, 783, L24
Zheng W. et al., 2013, ApJ, 778, L15

Table 2.   KAIT Photometry

| MJD | Filter | Magnitude |
|---|---|---|
| 56679.369 | B | 12.966 (022) |
| 56680.366 | B | 12.695 (012) |
| 56682.328 | B | 12.329 (009) |
| 56683.374 | B | 12.209 (008) |
| 56684.357 | B | 12.105 (010) |
| 56689.393 | B | 11.888 (011) |
| 56690.301 | B | 11.860 (008) |
| 56700.431 | B | 12.408 (019) |
| 56701.304 | B | 12.426 (018) |
| 56702.293 | B | 12.513 (019) |
| 56703.344 | B | 12.625 (013) |
| 56705.331 | B | 12.850 (010) |
| 56706.322 | B | 12.932 (009) |
| 56708.267 | B | 13.105 (011) |
| 56709.340 | B | 13.208 (009) |
| 56710.291 | B | 13.280 (022) |
| 56711.248 | B | 13.347 (014) |
| 56712.256 | B | 13.442 (016) |
| 56713.295 | B | 13.539 (017) |
| 56714.260 | B | 13.607 (036) |
| 56719.365 | B | 14.073 (014) |
| 56721.273 | B | 14.181 (015) |
| 56723.249 | B | 14.296 (011) |
| 56724.248 | B | 14.335 (013) |
| 56725.249 | B | 14.361 (025) |
| 56727.252 | B | 14.341 (027) |
| 56728.222 | B | 14.425 (015) |
| 56729.271 | B | 14.527 (014) |
| 56730.236 | B | 14.549 (016) |
| 56731.272 | B | 14.596 (017) |
| 56733.285 | B | 14.603 (018) |
| 56735.279 | B | 14.680 (016) |
| 56737.249 | B | 14.722 (045) |
| 56739.286 | B | 14.727 (013) |
| 56740.261 | B | 14.716 (020) |
| 56741.243 | B | 14.768 (015) |
| 56744.316 | B | 14.779 (036) |
| 56753.275 | B | 14.976 (017) |
| 56755.258 | B | 14.942 (019) |
| 56757.254 | B | 14.973 (018) |
| 56759.269 | B | 15.049 (143) |
| 56761.290 | B | 15.044 (018) |
| 56763.278 | B | 15.060 (022) |
| 56765.254 | B | 15.074 (018) |
| 56767.262 | B | 15.055 (020) |
| 56679.369 | V | 11.721 (018) |
| 56680.367 | V | 11.482 (013) |
| 56682.329 | V | 11.129 (013) |
| 56683.375 | V | 11.000 (012) |
| 56684.358 | V | 10.892 (012) |
| 56689.394 | V | 10.621 (017) |
| 56690.301 | V | 10.601 (012) |
| 56700.428 | V | 10.975 (037) |
| 56701.304 | V | 10.948 (018) |
| 56702.293 | V | 10.996 (024) |
| 56703.345 | V | 11.104 (013) |
| 56705.332 | V | 11.228 (014) |
| 56706.323 | V | 11.280 (012) |

Table 2 (cont'd)

| MJD | Filter | Magnitude |
|---|---|---|
| 56708.266 | *V* | 11.330 (012) |
| 56709.341 | *V* | 11.390 (012) |
| 56710.292 | *V* | 11.412 (026) |
| 56711.248 | *V* | 11.430 (016) |
| 56712.257 | *V* | 11.469 (025) |
| 56713.296 | *V* | 11.517 (022) |
| 56714.261 | *V* | 11.565 (021) |
| 56719.366 | *V* | 11.848 (014) |
| 56721.270 | *V* | 11.954 (017) |
| 56723.250 | *V* | 12.064 (009) |
| 56724.248 | *V* | 12.122 (011) |
| 56725.250 | *V* | 12.146 (018) |
| 56726.298 | *V* | 12.189 (139) |
| 56727.251 | *V* | 12.227 (008) |
| 56728.223 | *V* | 12.296 (008) |
| 56729.271 | *V* | 12.364 (012) |
| 56730.236 | *V* | 12.393 (011) |
| 56731.273 | *V* | 12.457 (016) |
| 56733.285 | *V* | 12.490 (013) |
| 56735.280 | *V* | 12.580 (014) |
| 56737.250 | *V* | 12.671 (024) |
| 56739.287 | *V* | 12.706 (011) |
| 56740.260 | *V* | 12.688 (011) |
| 56741.244 | *V* | 12.752 (011) |
| 56744.317 | *V* | 12.820 (018) |
| 56753.276 | *V* | 13.115 (018) |
| 56755.258 | *V* | 13.140 (010) |
| 56757.254 | *V* | 13.184 (017) |
| 56759.268 | *V* | 13.252 (042) |
| 56761.291 | *V* | 13.308 (011) |
| 56763.279 | *V* | 13.356 (014) |
| 56765.255 | *V* | 13.377 (009) |
| 56767.262 | *V* | 13.373 (013) |
| 56679.370 | *R* | 11.105 (021) |
| 56680.367 | *R* | 10.859 (013) |
| 56682.329 | *R* | 10.527 (016) |
| 56683.375 | *R* | 10.412 (020) |
| 56684.358 | *R* | 10.331 (017) |
| 56689.394 | *R* | 10.141 (018) |
| 56690.302 | *R* | 10.124 (012) |
| 56700.418 | *R* | 10.536 (025) |
| 56701.306 | *R* | 10.591 (024) |
| 56702.294 | *R* | 10.652 (030) |
| 56703.346 | *R* | 10.735 (017) |
| 56705.332 | *R* | 10.816 (017) |
| 56706.323 | *R* | 10.846 (017) |
| 56708.267 | *R* | 10.827 (015) |
| 56709.341 | *R* | 10.863 (014) |
| 56710.292 | *R* | 10.839 (029) |
| 56711.249 | *R* | 10.832 (021) |
| 56712.258 | *R* | 10.841 (031) |
| 56713.296 | *R* | 10.871 (031) |
| 56714.261 | *R* | 10.902 (022) |
| 56719.364 | *R* | 11.064 (013) |
| 56721.271 | *R* | 11.158 (020) |
| 56723.251 | *R* | 11.269 (009) |
| 56724.249 | *R* | 11.336 (015) |
| 56725.250 | *R* | 11.369 (021) |

Table 2 (cont'd)

| MJD | Filter | Magnitude |
|---|---|---|
| 56726.298 | *R* | 11.374 (094) |
| 56727.252 | *R* | 11.456 (008) |
| 56728.224 | *R* | 11.562 (007) |
| 56729.272 | *R* | 11.614 (010) |
| 56730.237 | *R* | 11.662 (012) |
| 56731.274 | *R* | 11.739 (021) |
| 56733.286 | *R* | 11.779 (016) |
| 56735.281 | *R* | 11.874 (017) |
| 56737.250 | *R* | 11.984 (026) |
| 56739.287 | *R* | 12.030 (015) |
| 56740.260 | *R* | 12.040 (012) |
| 56741.244 | *R* | 12.103 (018) |
| 56744.318 | *R* | 12.178 (024) |
| 56753.277 | *R* | 12.505 (014) |
| 56755.259 | *R* | 12.542 (014) |
| 56757.255 | *R* | 12.608 (019) |
| 56759.269 | *R* | 12.679 (036) |
| 56761.291 | *R* | 12.737 (012) |
| 56763.280 | *R* | 12.807 (024) |
| 56765.256 | *R* | 12.819 (010) |
| 56767.263 | *R* | 12.824 (013) |
| 56679.370 | *I* | 10.626 (026) |
| 56680.367 | *I* | 10.358 (015) |
| 56682.330 | *I* | 10.041 (021) |
| 56683.376 | *I* | 9.911 (024) |
| 56684.359 | *I* | 9.833 (021) |
| 56689.395 | *I* | 9.768 (025) |
| 56690.302 | *I* | 9.787 (014) |
| 56700.418 | *I* | 10.302 (042) |
| 56701.302 | *I* | 10.298 (030) |
| 56702.296 | *I* | 10.337 (037) |
| 56703.346 | *I* | 10.380 (021) |
| 56705.333 | *I* | 10.388 (018) |
| 56706.324 | *I* | 10.390 (025) |
| 56708.267 | *I* | 10.307 (015) |
| 56709.341 | *I* | 10.291 (016) |
| 56710.293 | *I* | 10.231 (034) |
| 56711.249 | *I* | 10.223 (022) |
| 56712.258 | *I* | 10.204 (033) |
| 56713.297 | *I* | 10.188 (034) |
| 56714.262 | *I* | 10.173 (026) |
| 56719.365 | *I* | 10.160 (019) |
| 56721.271 | *I* | 10.210 (030) |
| 56723.251 | *I* | 10.298 (013) |
| 56724.249 | *I* | 10.369 (018) |
| 56725.251 | *I* | 10.443 (025) |
| 56726.305 | *I* | 10.518 (079) |
| 56727.252 | *I* | 10.586 (009) |
| 56728.224 | *I* | 10.651 (007) |
| 56729.272 | *I* | 10.720 (012) |
| 56730.237 | *I* | 10.780 (013) |
| 56731.274 | *I* | 10.851 (025) |
| 56733.286 | *I* | 10.925 (019) |
| 56735.281 | *I* | 11.072 (020) |
| 56737.251 | *I* | 11.174 (032) |
| 56739.288 | *I* | 11.277 (022) |
| 56740.260 | *I* | 11.273 (013) |
| 56741.245 | *I* | 11.369 (022) |

Table 2  (cont'd)

| MJD | Filter | Magnitude |
|---|---|---|
| 56744.318 | *I* | 11.484 (026) |
| 56753.277 | *I* | 11.921 (020) |
| 56755.259 | *I* | 11.990 (018) |
| 56757.255 | *I* | 12.068 (023) |
| 56759.271 | *I* | 12.164 (056) |
| 56761.292 | *I* | 12.224 (015) |
| 56763.280 | *I* | 12.333 (024) |
| 56765.256 | *I* | 12.330 (015) |
| 56767.263 | *I* | 12.315 (022) |

Table 3.   FanCam Photometry

| UT (days) | *J* | *H* Magnitude | $K_s$ |
|---|---|---|---|
| 20140130.178 | 9.36 (02) | 9.44 (02) | 9.20 (01) |
| 20140201.101 | 9.51 (02) | 9.59 (02) | 9.38 (02) |
| 20140204.002 | 9.74 (01) | 9.67 (02) | 9.43 (02) |
| 20140208.096 | 10.03 (02) | 9.71 (02) | 9.47 (02) |
| 20140212.154 | 10.71 (01) | 9.77 (02) | 9.62 (02) |
| 20140220.101 | 10.89 (02) | 9.56 (02) | 9.48 (02) |
| 20140223.007 | 10.80 (02) | 9.49 (02) | 9.43 (02) |
| 20140225.004 | 10.68 (02) | 9.47 (02) | 9.35 (02) |
| 20140228.185 | 10.57 (02) | 9.57 (02) | 9.39 (02) |
| 20140401.600 | 11.80 (05) | 10.65 (07) | 10.74 (10) |
| 20140417.600 | 12.28 (05) | 11.02 (10) | 10.93 (10) |

Table 4.   Log of *HST*/STIS Spectral Observations

| Phase[a] | UT Date | Exposure[b](s) |
|---|---|---|
| −6.4 | 2014 Jan. 26.600 | 9573+300+200 |
| −4.6 | 2014 Jan. 28.443 | 4002+160+100 |
| −2.5 | 2014 Jan. 30.485 | 4002+160+100 |
| −0.4 | 2014 Feb. 1.610 | 4002+160+100 |
| +2.7 | 2014 Feb. 4.731 | 2255+160+100 |
| +6.5 | 2014 Feb. 8.525 | 4002+160+100 |
| +8.4 | 2014 Feb. 10.439 | 4002+160+100 |
| +11.3 | 2014 Feb. 13.293 | 4002+160+100 |
| +14.4 | 2014 Feb. 16.412 | 4002+160+100 |
| +24.1 | 2014 Feb. 26.069 | 11828+300+200 |

[a]Days since *B* maximum, 2014 Feb. 2.0 (JD 2,456,690.5).

[b]First, second, and third numbers correspond to the time for the G230L, G430L, and G750L gratings, respectively.

Table 5.    Log of IRTF/SpeX Spectral Observations

| Phase[a] | UT Date | Exposure[b](s) | SN 2014J Airmass | Standard | Standard Airmass |
|---|---|---|---|---|---|
| −7.5 | 2014 Jan. 25.45 | 720 | 1.58 | HIP52478 | 1.31 |
| −6.5 | 2014 Jan. 26.46 | 720 | 1.52 | HIP52478 | 1.30 |
| −5.6 | 2014 Jan. 27.42 | 960 | 1.64 | HIP52478 | 1.43 |
| −4.7 | 2014 Jan. 28.30 | 2000 | 2.45 | HIP45590 | 2.25 |
| −0.6 | 2014 Feb. 01.39 | 840 | 1.67 | HIP52478 | 1.45 |

[a]Days since $B$ maximum, 2014 Feb. 2.0 (JD 2,456,690.5).

Table 6.    Log of TRES Spectral Observations

| Phase[a] | UT Date | Exposure[b](s) |
|---|---|---|
| −10.6 | 2014 Jan. 23.399 | 1800 |
| −7.5 | 2014 Jan. 26.463 | 1200 |
| +7.3 | 2014 Feb. 10.323 | 1980 |
| +9.3 | 2014 Feb. 12.315 | 1800 |
| +11.3 | 2014 Feb. 14.329 | 1800 |
| +12.3 | 2014 Feb. 15.329 | 1800 |
| +15.4 | 2014 Feb. 18.413 | 1800 |
| +17.4 | 2014 Feb. 20.433 | 1920 |
| +41.2 | 2014 Mar. 16.243 | 1800 |
| +47.3 | 2014 Mar. 22.302 | 1000 |

[a]Days since $B$ maximum, 2014 Feb. 2.0 (JD 2,456,690.5).

Table 7.    Photometric Parameters

| Filter | $t_{\max}$ (MJD) | Maximum Brightness (mag) | $\Delta m_{15}$ (mag) | $A_X$[a] (mag) |
|---|---|---|---|---|
| F218W | 56689.3 (1) | 18.02 (03) | 0.99 (05) | $\cdots$ |
| F225W | 56688.4 (1) | 18.50 (03) | 0.85 (04) | $\cdots$ |
| F275W | 56687.6 (2) | 16.42 (03) | 1.65 (05) | $\cdots$ |
| F336W | 56687.2 (2) | 13.02 (03) | 1.62 (02) | $\cdots$ |
| $B$ | 56690.0 (2) | 11.85 (02) | 0.95 (01) | 3.38 (20) |
| $V$ | 56691.0 (6) | 10.61 (05) | 0.60 (01) | 2.07 (18) |
| $R$ | 56690.9 (8) | 10.12 (07) | 0.69 (03) | 1.65 (18) |
| $I$ | 56688.1 (9) | 9.75 (10) | 0.62 (07) | 1.07 (21) |
| $J$ | <56687.2 | <9.36 | $\cdots$ | 0.26 (21) |
| $H$ | $\lesssim$56687.2 | $\lesssim$9.44 | $\cdots$ | 0.13 (16) |
| $K_s$ | $\lesssim$56687.2 | $\lesssim$9.20 | $\cdots$ | 0.00 (23) |

[a]As determined relative to the Prieto et al. (2006) templates for the optical bands and average of the methods listed by Matheson et al. (2012) for the NIR bands. Includes a 0.10 mag distance uncertainty to M82.

Table 8. Synthesised SN 2011fe UV Photometry

| MJD | Filter | Magnitude[a] |
|---|---|---|
| 55801.174 | F218W | 17.35 |
| 55804.270 | F218W | 15.51 |
| 55807.431 | F218W | 14.02 |
| 55811.423 | F218W | 13.37 |
| 55814.440 | F218W | 13.20 |
| 55817.677 | F218W | 13.11 |
| 55823.630 | F218W | 14.08 |
| 55835.269 | F218W | 15.46 |
| 55841.320 | F218W | 15.85 |
| 55855.203 | F218W | 16.39 |
| 55801.174 | F225W | 16.86 |
| 55804.270 | F225W | 14.69 |
| 55807.431 | F225W | 13.24 |
| 55811.423 | F225W | 12.73 |
| 55814.440 | F225W | 12.65 |
| 55817.677 | F225W | 12.74 |
| 55823.630 | F225W | 13.57 |
| 55835.269 | F225W | 14.95 |
| 55841.320 | F225W | 15.35 |
| 55855.203 | F225W | 15.95 |
| 55801.174 | F275W | 14.62 |
| 55804.270 | F275W | 12.28 |
| 55807.431 | F275W | 11.05 |
| 55811.423 | F275W | 10.73 |
| 55814.440 | F275W | 10.82 |
| 55817.677 | F275W | 11.18 |
| 55823.630 | F275W | 12.16 |
| 55835.269 | F275W | 13.71 |
| 55841.320 | F275W | 14.19 |
| 55855.203 | F275W | 14.83 |
| 55801.174 | F336W | 12.52 |
| 55804.270 | F336W | 10.49 |
| 55807.431 | F336W | 9.55 |
| 55811.423 | F336W | 9.25 |
| 55814.440 | F336W | 9.33 |
| 55817.677 | F336W | 9.70 |
| 55823.630 | F336W | 10.63 |
| 55835.269 | F336W | 12.37 |
| 55841.320 | F336W | 12.95 |
| 55855.203 | F336W | 13.64 |

[a]Uncertainty in synthesised photometry is ∼0.1 mag.

Table 9. Spectral Phases (days relative to *B*-band maximum)

| SN 2014J | −6.4 | −4.6 | −2.5 | −0.4 | +2.7 | +6.5 | +8.4 | +11.3 | +14.4 | +24.1 |
|---|---|---|---|---|---|---|---|---|---|---|
| SN 2009ig | ⋯ | −4.2 | −2.1 | ⋯ | ⋯ | ⋯ | +8.5 | ⋯ | ⋯ | ⋯ |
| SN 2011fe | −6.9 | ⋯ | −3.0 | 0.0 | +3.2 | ⋯ | +9.1 | ⋯ | ⋯ | +26.7 |
| SN 2013dy | −6.2 | ⋯ | −2.1 | −0.4 | ⋯ | ⋯ | +8.8 | +12.4 | +14.4 | +21.2 |